High-resolution mapping reveals topologically distinct cellular pools of phosphatidylserine

Gregory D. Fairn,[1] Nicole L. Schieber,[2,3] Nicholas Ariotti,[2] Samantha Murphy,[2] Lars Kuerschner,[2] Richard I. Webb,[3] Sergio Grinstein,[1] and Robert G. Parton[2,3]

[1]Program in Cell Biology, Hospital for Sick Children, Toronto, Ontario, Canada M5G 1X8
[2]Institute for Molecular Bioscience and [3]Centre for Microscopy and Microanalysis, The University of Queensland, Queensland 4072, Australia

Phosphatidylserine (PS) plays a central role in cell signaling and in the biosynthesis of other lipids. To date, however, the subcellular distribution and transmembrane topology of this crucial phospholipid remain ill-defined. We transfected cells with a GFP-tagged C2 domain of lactadherin to detect by light and electron microscopy PS exposed on the cytosolic leaflet of the plasmalemma and organellar membranes. Cytoplasmically exposed PS was found to be clustered on the plasma membrane, and to be associated with caveolae, the trans-Golgi network, and endocytic organelles including intraluminal vesicles of multivesicular endosomes. This labeling pattern was compared with the total cellular distribution of PS as visualized using a novel on-section technique. These complementary methods revealed PS in the interior of the ER, Golgi complex, and mitochondria. These results indicate that PS in the lumenal monolayer of the ER and Golgi complex becomes exposed cytosolically at the trans-Golgi network. Transmembrane flipping of PS may contribute to the exit of cargo from the Golgi complex.

Introduction

Phospholipids serve a variety of regulatory and signaling functions in eukaryotic cells. Indeed, phosphoinositides are acknowledged to transduce key signals in a variety of organelles (Downes et al., 2005; Kutateladze, 2010). In addition, phosphatidylserine (PS) is recognized to play a central role in the recognition and clearance of apoptotic bodies and in blood coagulation. Within the cell, PS contributes to the recruitment and/or activation of proteins such as protein kinase C, synaptotagmin, and K-Ras (Vance, 2008; Yeung et al., 2009).

The function of PS is determined by its concentration and sidedness in the individual organelles. The subcellular distribution of PS is the result of the coordinated actions of metabolic enzymes in conjunction with vesicular and nonvesicular transport pathways, whereas PS flippases, floppases, and scramblases determine the transmembrane topology. Mitochondria-associated membranes have high rates of PS synthesis and serve as a conduit for the transfer of lipids between the ER and adjacent mitochondria (Ardail et al., 1991; Cui et al., 1993). Remarkably, the available determinations of PS, obtained by fractionation and chemical analysis, indicate that neither the ER nor the mitochondria are enriched in PS. In fact, the mole ratio of PS in the plasma membrane (PM) has been estimated to be ∼4- and 10-fold higher than that of the ER and mitochondria, respectively (van Meer et al., 2008). The PS content of less abundant organelles is less well defined because of the difficulty inherent in purifying them to homogeneity. Technical problems have also plagued the determination of PS topology, which has only been established with certainty for the PM, on account of its accessibility.

In view of the functional importance of PS, a more accurate definition of its subcellular distribution and transbilayer topology is required. Despite remarkable advances in lipid mass spectrometry, the reliance on cellular fractionation limits its usefulness in the assessment of subcellular distribution, and other methods must be applied instead. To this end, genetically encoded probes that bind specifically to PS were introduced recently (Yeung et al., 2008). They consist of discoidin-type C2 domains, which recognize PS stereospecifically in the absence of Ca^{2+}. These probes can be expressed in cells to determine the cytoplasmically accessible PS by light microscopy or EM. In addition, a recombinant probe synthesized in bacteria can be used to label lipids in a near-native state by overlaying otherwise

Correspondence to R.G. Parton: R.Parton@imb.uq.edu.au

Abbreviations used in this paper: FS, freeze substitution; HPF, high-pressure freezing; ILV, intraluminal vesicle; LTE, low-temperature embedding; MVB, multivesicular body; PLC, phospholipase Cδ; PM, plasma membrane; PS, phosphatidylserine; RER, rough endoplasmic reticulum.

The Rockefeller University Press $30.00
J. Cell Biol. Vol. 194 No. 2 257–275
www.jcb.org/cgi/doi/10.1083/jcb.201012028

untreated cells. For light microscopy of whole cultured cells, such an approach would require permeabilization protocols with potential problems of lipid removal, redistribution, or differential accessibility across different compartments. However, when combined with on-section labeling, as used for post-embedding immuno-EM, this problem can be avoided. Nevertheless, specific challenges are associated with lipid localization, as lipids are generally not well retained by conventional fixatives and by processing schemes that were developed for proteins rather than lipids. Rapid freezing avoids these problems but has to be combined with dehydration (usually freeze-substitution [FS]; i.e., dehydration at low temperature) and embedding in resin. Throughout this procedure, the lipids must be maintained in their native localization while retaining their accessibility to the overlaid probe (van Genderen et al., 1991; Voorhout et al., 1991; Möbius et al., 2002). The ideal processing and labeling scheme would minimize any perturbation of the cells before processing, would avoid lipid loss or redistribution during processing and labeling, and would allow labeling efficiencies similar to the protein localization methods currently in use.

Here, we used the C2 domain of lactadherin to generate chimeric constructs that could be expressed in cells for detection by fluorescence microscopy or EM. In addition, we provide quantitative information on PS distribution at the ultrastructural level based on a novel on-section labeling approach on fast-frozen materials with a purified C2 domain probe. These combined approaches yield unique information on the subcellular distribution, transmembrane topology, and domain segregation of PS.

Results

High-resolution analysis of intracellular PS distribution

A fusion of the C2 domain of lactadherin with GFP (GFP-Lact-C2) was used to visualize PS. When expressed in A431 cells, GFP-Lact-C2 decorates the cell periphery as well as internal organelles (Fig. 1 a). That the peripheral labeling reflects the presence of PS at the PM is indicated by the extensive overlap of GFP-Lact-C2 with an RFP-tagged pleckstrin homology (PH) domain of phospholipase Cδ (PLCδ), which binds to plasmalemmal phosphatidylinositol 4,5-bisphosphate (Fig. 1 a). Accordingly, mRFP-Lact-C2 was also found to colocalize with Alexa Fluor 488–conjugated cholera toxin B, which binds to the exofacial ganglioside, GM1 (Fig. 1 a).

Next, we used EM to localize the expressed probe at the ultrastructural level. BHK cells were transfected with GFP-Lact-C2 and then fixed and processed for frozen sections according to standard methods (Slot and Geuze, 2007). The expressed probe was localized using antibodies to GFP, followed by protein A–gold. Consistent with earlier studies using RAW264.7 macrophages (Yeung et al., 2008) and with biochemical determinations indicating that PS is enriched in the PM, dense labeling for the PS probe was associated with the PM (e.g., Figs. 1 b and 2 a). Remarkably, even at very high expression levels, negligible cytosolic labeling was detectable, and other compartments, such as the ER, showed extremely low labeling (Figs. 1, 2, and 6).

Ultrastructural analysis of PM PS distribution

Having validated the usefulness of the Lact-C2 domain for EM, we took advantage of the enhanced spatial resolution of this method to analyze the nanoscale distribution of PS. The possibility that lipids may segregate in the plane of the membrane has garnered much interest in recent years. Thus, cholesterol and sphingolipid-enriched "rafts" are thought to play unique functions in transport and signal transduction (Lingwood and Simons, 2010). The majority of cellular PS molecules contain unsaturated acyl chains, which are not conducive to partitioning in rafts (Keenan and Morré, 1970; van Meer, 1998). However, a subpopulation of PS molecules acylated with saturated chains may associate with cholesterol and sphingolipid-enriched microdomains (Pike et al., 2005). To assess this possibility, we studied the distribution of PS in the inner leaflet of the PM by preparing PM lawns from BHK cells expressing GFP-Lact-C2. The lawns were fixed with a glutaraldehyde-containing fixative within seconds of cell disruption and then labeled with anti-GFP gold complexes and analyzed exactly as described previously (Fig. 1, f and g; Prior et al., 2003; Plowman et al., 2005). K-function analysis to assess deviations from spatial homogeneity showed significant clustering of PS, with a peak at ∼22 nm (Fig. 1 g, inset). Using previously described calibration of anti-GFP labeling in the same experimental system (Plowman et al., 2005), this suggests association of PS with microdomains of ∼11 nm in diameter. In addition, significant labeling of 60–80-nm vesicular profiles with the morphology of caveolae was observed (Fig. 1 g). Consistent with this, immuno-EM analysis of sectioned low-expressing cells labeled for the caveolar coat protein, cavin-1/PTRF, showed substantial labeling with GFP-Lact-C2 in regions enriched in caveolae (Fig. 1, c–e). The plasmalemmal clustering and enrichment of PS in caveolae is not a general feature of sites of endocytosis. Indeed, we did not detect preferential accumulation of PS in clathrin-coated pits using either total internal reflection fluorescence microscopy or by immuno-EM analysis of cells transfected (unpublished data).

PS in the endoplasmic reticulum: development of on-section labeling methods for PS

PS content of the ER is markedly lower than that of the PM (van Meer et al., 2008). We verified this finding in A431 cells transfected with mRFP-Lact-C2; the fluorescent PS probe was not detectable in membranes identified as ER by labeling with GFP-KDEL or Sec61α-GFP (Fig. 2 a). Furthermore, immunogold analysis of cells expressing GFP-Lact-C2 showed sparse labeling in the ER compared with that seen in the PM (Figs. 1, 2, and 6; PM gold density, 14.7 gold particles per μm; ER, 0.048 gold particles per μm; i.e., PM/ER ratio > 300). Assuming a typical labeling efficiency for frozen sections of 5% and a section thickness of 60 nm (see Materials and methods), the PM labeling density observed would be equivalent to $\sim 1.10^7$ PS molecules in the PM of one cell.

The failure of the C2 domain probes to associate detectably with the ER is remarkable, considering that PS is generated in this compartment. It is conceivable that the phospholipid is

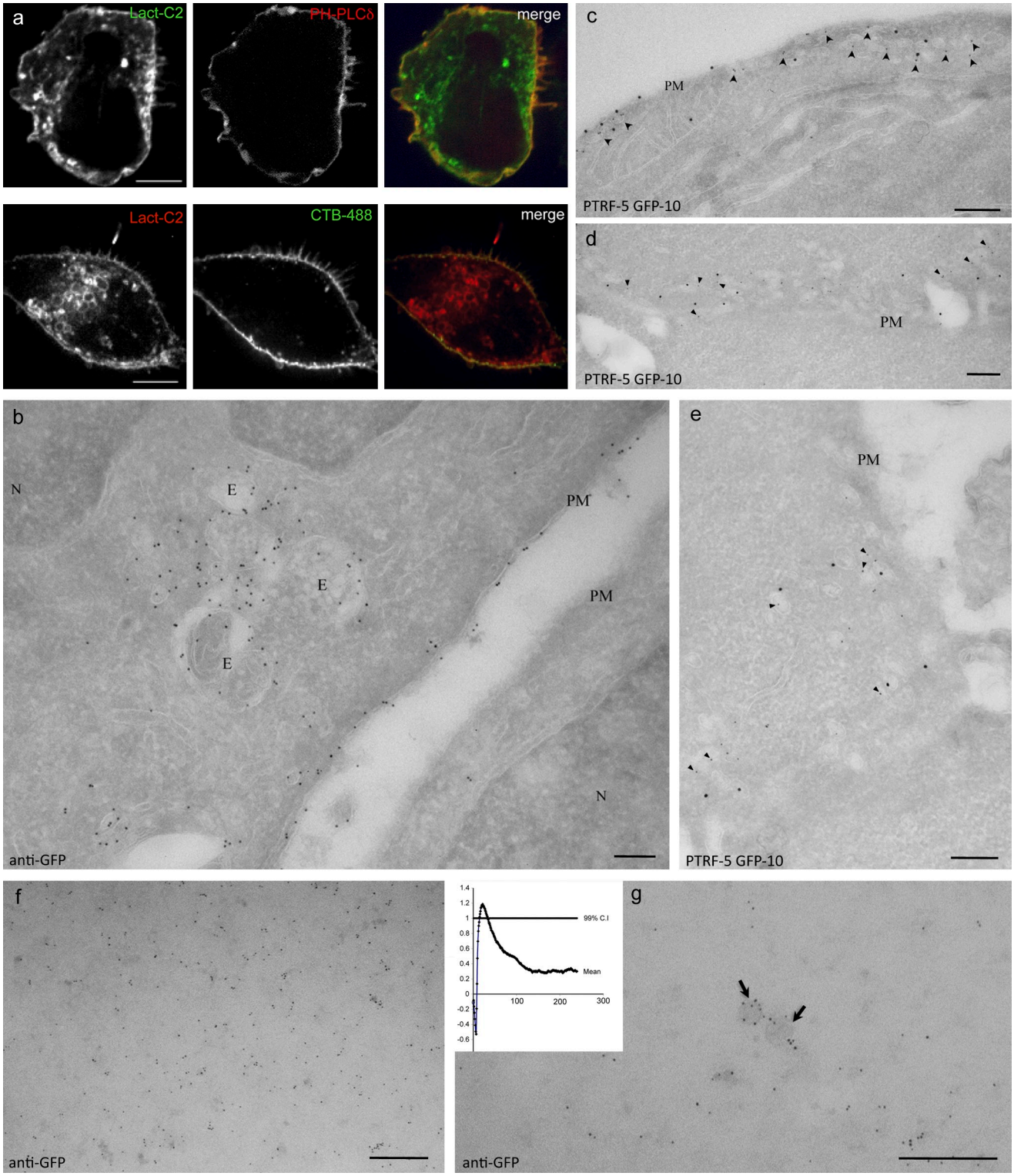

Figure 1. **Plasma membrane localization of expressed GFP-Lact-C2.** (a, top) A431 cells cotransfected with GFP-Lact-C2 (left) and RFP-PH-PLCδ (middle), as well as a merged image (right). (a, bottom) A431 cells transfected with mRFP-Lact-C2 and stained with Alexa Fluor 488–labeled cholera Toxin B. (b) Representative frozen section of cells expressing GFP-Lact-C2 and immunogold labeled for the GFP tag. Note labeling over the PM of the expressing cell, but not the neighboring cell, and the lack of cytosolic labeling. The nucleus (N) and nuclear envelope are unlabeled but multivesicular endosomes (E) show significant labeling. (c–e) Cells transfected with GFP-Lact-C2 double labeled for PTRF/cavin-1 (small gold) and GFP (large gold). Note the significant labeling for GFP in the regions enriched in PTRF/cavin-1–labeled caveolae (arrowheads). (f and g) PM lawns were prepared from GFP-Lact-C2–transfected cells and labeled with anti-GFP antibody gold conjugates. GFP-Lact-C2 is clustered in undifferentiated regions of the PM (f) and also labels vesicular profiles (g). Arrows indicate membrane domains consistent with caveolae. Cluster analysis suggests peak clustering at ~22 nm (inset). Bars: (b–g) 200 nm.

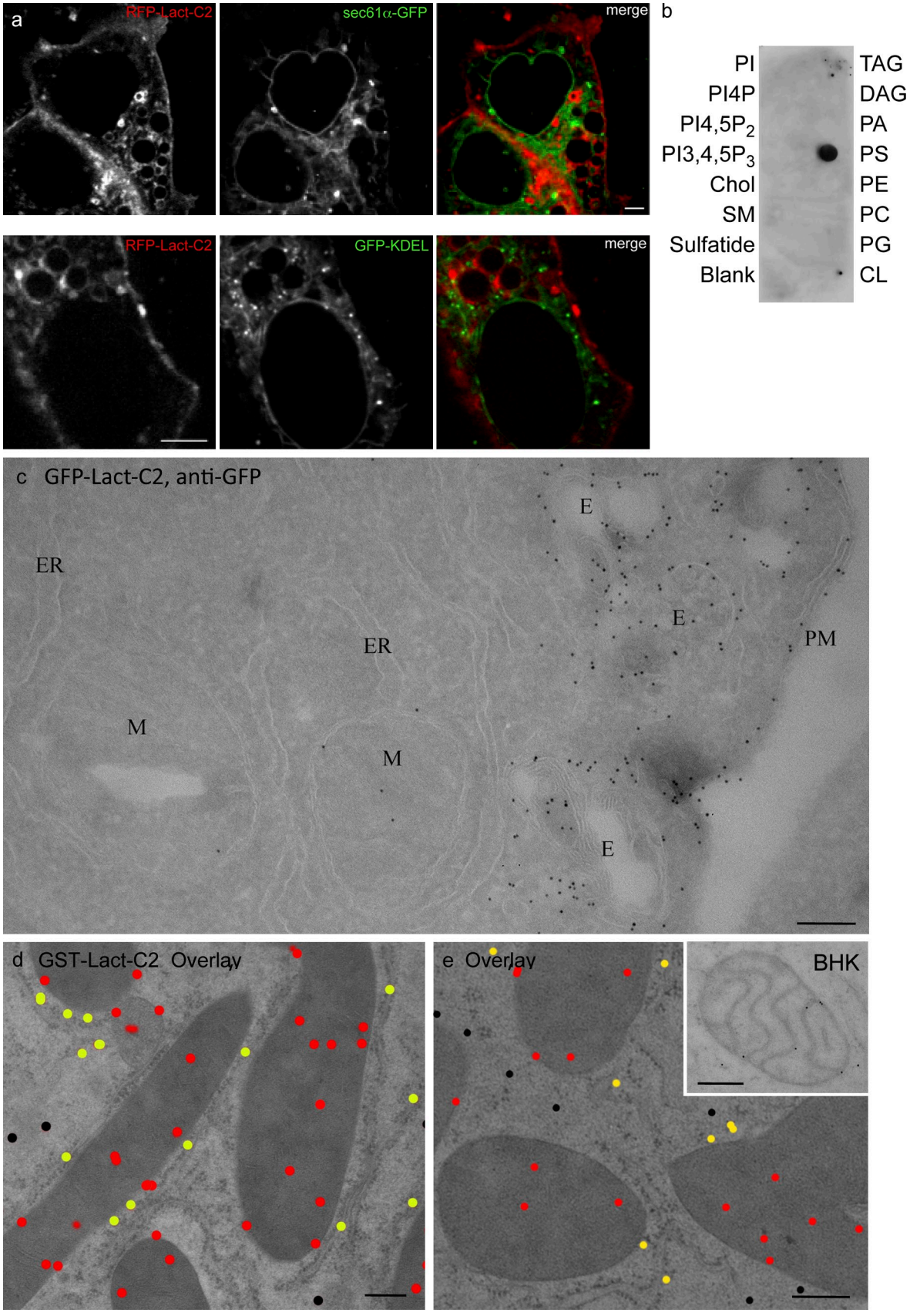

Figure 2. **Comparison of expressed GFP-LactC2 with postprocessing immunolabeling.** (a, top) A431 cells cotransfected with mRFP-Lact-C2 (left) and sec61α-GFP (middle). The images are overlaid on the right. (a, bottom) A431 cells cotransfected with mRFP-Lact-C2 and GFP-KDEL. (b) Binding specificity of GST-Lact-C2: overlay assays were performed using lipid strips from Echelon. PA, phosphatidic acid; PC, phosphatidylcholine; PE, phosphatidylethanolamine;

Table I. **Labeling density with the C2 probe on different organelles**

Tissue/cell compartment	C2	GST	Ratio C2/GST	Ratio PM/X
Liver PM	4.03 ± 0.27	0.14 ± 0.002	29.1	1
Liver RER	0.96 ± 0.24	0.058 ± 0.0075	16.6	4.2
Liver mitochondria	0.82 ± 0.04	0.049 ± 0.0035	16.9	4.9
Liver mitochondria (volume)[a]	11 ± 1.54	0.058 ± 0.0075	16.9	NA
A431 PM	7.65 ± 0.78	0.19 ± 0.005	41.4	1
A431 RER	2.12 ± 0.21	0.090 ± 0.03	23.6	3.6
A431 Golgi	2.62	0.08	32.8	2.9
A431 Endosome[b]	3.34	0	NA	2.3

Units of measure are given in gold/μm ± SEM unless otherwise indicated.
[a]Gold/μm^2± SEM.
[b]Limiting membrane only.

rapidly exported from the ER to other organelles. Alternatively, PS may be translocated to the lumenal monolayer, where it would be inaccessible to the cytosolic Lact-C2 probe. Indeed, lipids synthesized in the cytosolic leaflet are flipped to the lumenal monolayer to facilitate proper expansion of the ER, although the resulting transbilayer distribution is the subject of debate (Bell et al., 1981; Zachowski, 1993). However, when expressed in the cytosol, the GFP-Lact-C2 probe can only gain access to PS exposed on the cytoplasmic leaflet of cellular membranes. To overcome this limitation, we developed an on-section approach using a purified Lact-C2 fusion protein. To facilitate purification and detection, the recombinant C2 domain was fused to GST, which served as an epitope for immunogold labeling. The effectiveness and specificity of the GST-Lact-C2 fusion protein was validated using a lipid overlay assay. As shown in Fig. 2 b, only PS interacted with the fusion construct, whereas other lipids remained unlabeled. The latter included several anionic phospholipids, which implies that the interaction of the probe with PS is stereospecific and not merely electrostatic, which is consistent with previous studies (Shi et al., 2004; Shao et al., 2008).

We next tested whether GST-Lact-C2 could be used to detect PS on ultrathin sections overlaid with the probe. Importantly, this method avoids the use of detergent extraction or cell permeabilization, providing access to the entire pool of PS, including the lumen of all organelles exposed on the surface of the section. Labeling with the PS probe on conventional frozen sections proved to be unsuccessful, with negligible PM labeling and redistribution of PS (Fig. S2), as seen with other lipid probes (Liou et al., 1996). We therefore validated the use of a technique which involves high-pressure freezing (HPF) to avoid a primary fixation step, FS with medium containing minimal levels of fixative (only 0.2% uranyl acetate), and embedding at low temperature (−45°C) in a UV-polymerized resin (low-temperature embedding [LTE]; Nixon et al., 2009; Schieber et al., 2010). After incubation with the probe on ice, sections were fixed and the probe was detected with anti-GST antibodies, followed by 10 nm protein A–gold.

We first performed a detailed comparison of the labeling obtained with wild-type GST-Lact-C2, GST alone, or the binding-deficient mutant GST-Lact-$C2^{(W26A,W33A,F34A)}$ (Shao et al., 2008). As shown in Figs. 2, 3, S2, and S3, the GST-Lact-C2 probe showed specific labeling of mitochondria, ER, PM, and endocytic compartments. A consistently high signal-to-noise ratio was obtained in all the cells and tissues examined to date (the ratio of labeling with GST-Lact-C2 probe/GST was 41.4 for the PM of A431 cells, 29.1 for the liver PM, and 16.7 for liver rough endoplasmic reticulum [RER]; Table I). In addition, there was little evidence of lipid redistribution in frozen sections (compare Figs. S2 a with S2 b and S2 d). In cultured cells, some labeling, presumably representing lipids that have redistributed from the PM during processing, was evident in some areas, but generally the retention of PM PS was extremely good, as indicated by the clearly defined restriction of labeling to the PM (Figs. 3, S2, and S3). Consistent with analysis of cells expressing the GFP-Lact-C2 probe, high labeling was particularly apparent in areas rich in caveolae (Fig. S3).

Sections of mouse liver (Figs. 2 and 3), BHK cells (Figs. 2, 4 and S2), A431 cells (Figs. 3 and 4), differentiated 3T3L1 adipocytes (Fig. S3), and zebrafish embryos (not depicted) were prepared using the HPF/FS/LTE scheme and labeled with the GST-Lact-C2 probe. In addition to the strong labeling of the PM (mean gold particles/μm ± SEM; liver PM, 4.03 ± 0.26; A431 PM, 7.65 ± 0.19) and in contrast to the cytosolically expressed probes, the overlaid GST-Lact-C2 consistently labeled the ER in all tissues tested (liver RER, 0.96 ± 0.24; A431 RER, 2.12 ± 0.21). The ratio of PM/ER labeling ranged from 4.2 (liver) to 3.6 (A431). The greater density of label when both sides of the membrane are accessible suggests that PS is preferentially

PG, phosphatidylglycerol; PI, phosphatidylinositol; SM, sphingomyelin; TAG, triacylglycerol. (c) BHK cells transiently transfected with GFP-Lact-C2, frozen sectioned, and stained using anti-GFP antibody followed by incubation with gold-labeled protein A. Note the labeling of the PM and endosomes (E), but negligible labeling of ER and mitochondria (M). (d and e) Mouse liver samples or BHK cells (inset) were high pressure-frozen, freeze-substituted, and embedded in UV-polymerized Lowicryl at low temperature. Sections were incubated with purified GST-Lact-C2 and labeled as described in Materials and methods. Images were pseudocolored to highlight gold particles, which were color-coded to indicate assignment to specific compartments: red, mitochondria; yellow, RER; black, unassigned. Note the labeling of mitochondria, including cristae (inset), and the RER, particularly in close apposition to the ER. Unmodified images of d and e are provided in Fig. S5. Bars: (a) 4 μm; (c–e) 200 nm.

localized to the inner leaflet of the ER. Note that assignment of gold particles to the lumenal or cytoplasmic aspect of the membrane is difficult by immuno-EM because of the large distance from the antigen to the gold particle (including the probe, primary antibody, and protein A–gold) relative to the ~4 nm bilayer and the apparent random orientation of the complex relative to the antigen. However, comparison of labeling with the cytoplasmic probe and the on-section probe provides compelling support for this model, which is consistent with earlier determinations of PS latency using lipases (Higgins and Dawson, 1977; Dominski et al., 1983), though not with all studies (Sundler et al., 1977).

Ultrastructural examination using the GST-Lact-C2 overlay method also allowed us to visualize the regions of the ER in close proximity to the mitochondria. Using thin sections of liver cells, we noted significant labeling of PS in regions of the ER proximal to mitochondria (Fig. 2 d).

Ultrastructural detection of an internal pool of mitochondrial PS

As reported for macrophages (Yeung et al., 2008), expression of GFP-Lact-C2 failed to label the mitochondria, which were identified by co-expression of the mito-RFP construct. This is apparent in Fig. 3 a, as well as from a Manders scatter plot, where the correlation between red and green pixel location was analyzed. This analysis yielded a Manders overlap coefficient (M) of 0.1 ± 0.01, which is statistically insignificant ($P > 0.1$) and suggestive of mutually exclusive staining. Immunogold staining and EM analysis of cells expressing GFP-Lact-C2 also showed very low mitochondrial labeling (Fig. 2 c). These results imply that there is little PS in the cytosolic leaflet of the outer mitochondrial membrane, despite the proximity of the mitochondria-associated membranes. This may reflect the rapid decarboxylation of PS to phosphatidylethanolamine by the mitochondria. However, inaccessibility of the cytosolically expressed probe may also account for the observations. Indeed, the sole PS decarboxylase of mammalian cells resides in the inner membrane of the mitochondrion, which suggests that PS is directed to this inaccessible compartment. This possibility was assessed by EM using the post-sectioning overlay technique. As in the previous section, mouse liver, 3T3-L1 adipocytes, or cultured cell (BHK or A431) sections were incubated with purified GST-Lact-C2, followed by staining with anti-GST antibody and protein A–gold. Under these conditions, significant PS was detectable on mitochondrial profiles (liver mitochondria gold particles/μm^2; GFP-Lact-C2 probe, 11.0 ± 1.54; GST, 1.73 ± 0.13) with labeling on cristae and around the periphery of the mitochondria (Figs. 2 and 3; 0.82 ± 0.04 particles/μm of the mitochondrial outer membrane).

PS is present throughout the Golgi complex but exposed to the cytosolic leaflet only in the trans-Golgi network

The Golgi complex serves as a major cargo-sorting station, contributing to generate and maintain differences in protein and lipid profiles between the ER, the PM, and the endocytic pathway. In yeast (Chen et al., 1999; Hua et al., 2002), and likely also in mammalian cells, the Golgi complex is in addition an important repository of flippases that establish the transmembrane asymmetry of aminophospholipids, including PS. This prompted us to examine the distribution of PS in the Golgi complex by a combination of fluorescence and EM.

In mammalian cells, the Golgi apparatus is composed of a juxtanuclear stack of cisternae that are in a dynamic steady state. To assess the appearance of PS along this stage of the secretory pathway, we expressed resident markers of individual subcompartments of the Golgi complex, together with Lact-C2 conjugated to either green or red fluorescent proteins, as appropriate. The cells were analyzed by spinning-disc microscopy, and the degree of overlap of the probes was calculated. HeLa cells were transfected with galactosyl-transferase tagged with GFP (GalT-GFP), which is present predominantly in the trans-Golgi cisternae and to a lesser extent in the TGN (Rabouille et al., 1995; Mironov et al., 2001), together with RFP-Lact-C2 (Fig. 4 a). Only modest colocalization of GalT-GFP with mRFP-Lact-C2 is seen (M_{green} = 0.41 ± 0.05; $P > 0.1$). To more selectively establish the presence of PS on the cytosolic leaflet of the TGN, HeLa cells were transfected with RFP-Lact-C2, fixed, permeabilized and stained with antibodies to TGN46 (Fig. 4 a). TGN46, a specific marker of the TGN (Prescott et al., 1997), overlapped extensively with RFP-Lact-C2 (M_{green} = 0.77 ± 0.05; $P < 0.01$), which is consistent with PS being exposed to the cytosol in this compartment. Similar results were observed in A431 cells, which suggests that, like yeast, mammalian cells have one or more aminophospholipid flippases located in the trans-Golgi or, more likely, the TGN (Fig. S4). Immuno-EM localization of expressed GFP-Lact-C2 was in full agreement with these observations. Specific labeling for the expressed protein was concentrated on membranous elements close to the Golgi stack shown to be the TGN by colocalization with the Golgin GCC-88 (Luke et al., 2003), but rarely on Golgi cisternae (Fig. 4, e and f). In contrast, labeling of endogenous PS by overlaying sections revealed more uniform labeling throughout the Golgi complex, including Golgi cisternae (Fig. 4, b–d). Quantitation showed 49.8 ± 2.2% (mean ± SEM, $n = 14$) of labeling associated with Golgi cisternae, expressed as the percentage of total Golgi-associated labeling, when using the overlay technique, as compared with 8.4 ± 1.7% ($n = 12$) with the cytoplasmically expressed probe. These results suggest that cytoplasmic exposure of PS occurs in, or close to, the TGN.

Recycling endosomes interact extensively with the TGN, and the two compartments are therefore expected to share structural features. We tested this notion by labeling recycling endosomes with rhodamine-conjugated transferrin (Rhod-Trfn). HeLa cells were chosen for these and the preceding experiments because their recycling endosomes, unlike those of A431 cells, cluster discretely in the immediate vicinity of the TGN (Fig. 4 a), and are therefore more accurately quantified. A considerable degree of overlap was found between Rhod-Trfn and GFP-Lact-C2 (M_{Red} = 0.81 ± 0.05; $P < 0.01$), which indicates abundant exposure of PS on the cytosolic leaflet of recycling endosomes.

Localization of PS on the limiting membrane and internal vesicles of multivesicular endosomes

Despite continuous delivery of vesicular material between compartments of the endocytic pathways, large differences in PS

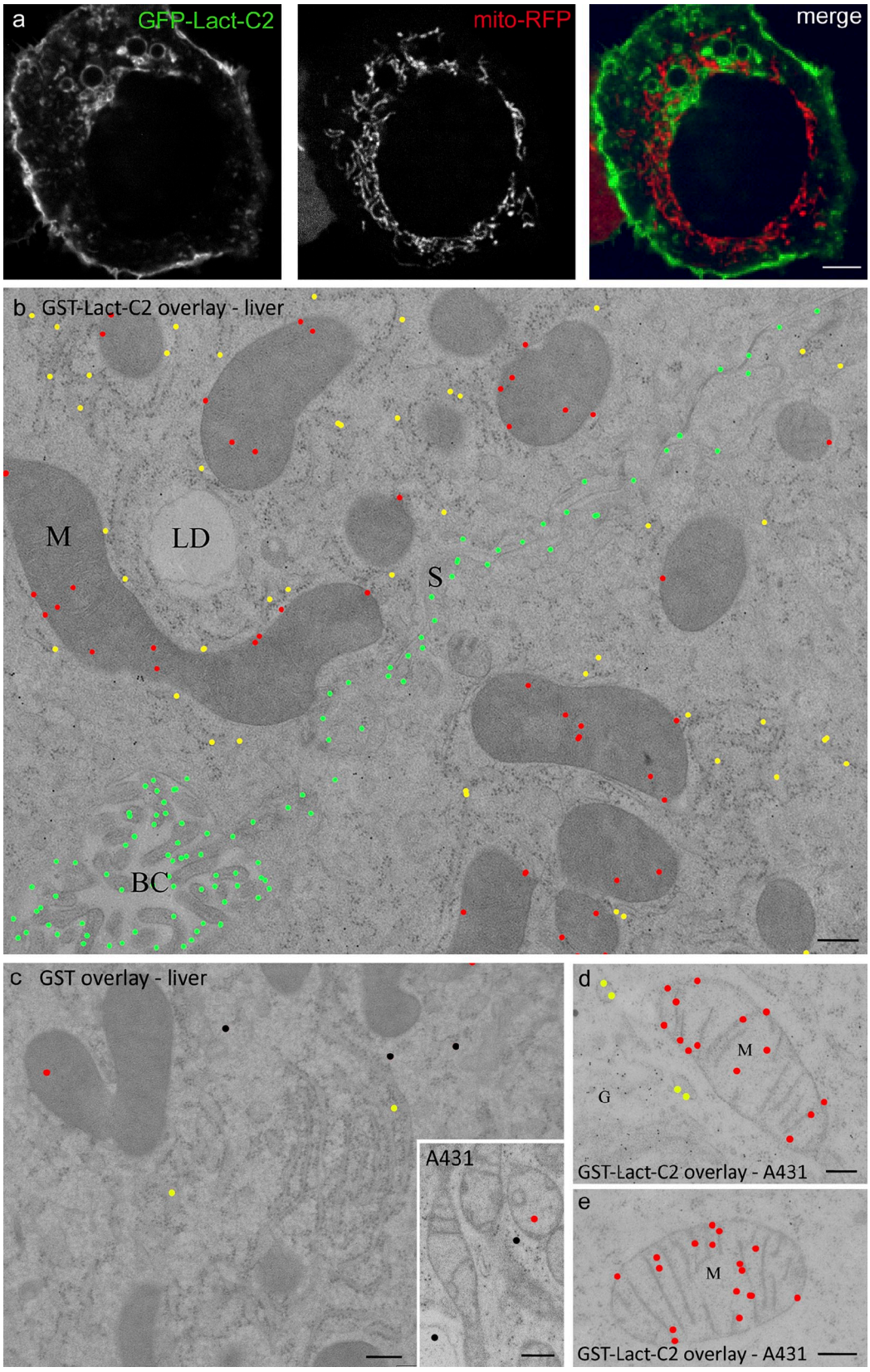

Figure 3. **On-section ultrastructural localization of PS.** (a) A431 cells transiently cotransfected with GFP-Lact-C2 (left) and mito-RFP (middle). The images are overlaid on the right. (b–e) Mouse liver (b and c) and A431 samples (d and e) were processed using HPF/FS/LTE. Sections were incubated with purified GST-Lact-C2 (b, d, and e) or with GST (c and inset) and labeled as described in Materials and methods. Images were color-coded to indicate specific compartments: green, PM; red, mitochondria; yellow, RER; black, unassigned. Note the specific labeling of mitochondria, the RER, and the PM with GST-Lact-C2, compared with GST alone. Unmodified images of b–e are provided in Fig. S5. G, Golgi complex; LD, lipid droplet; S, sinusoidal membrane; BC, bile canaliculus. Bars: (a) 4 µm; (b–e) 200 nm.

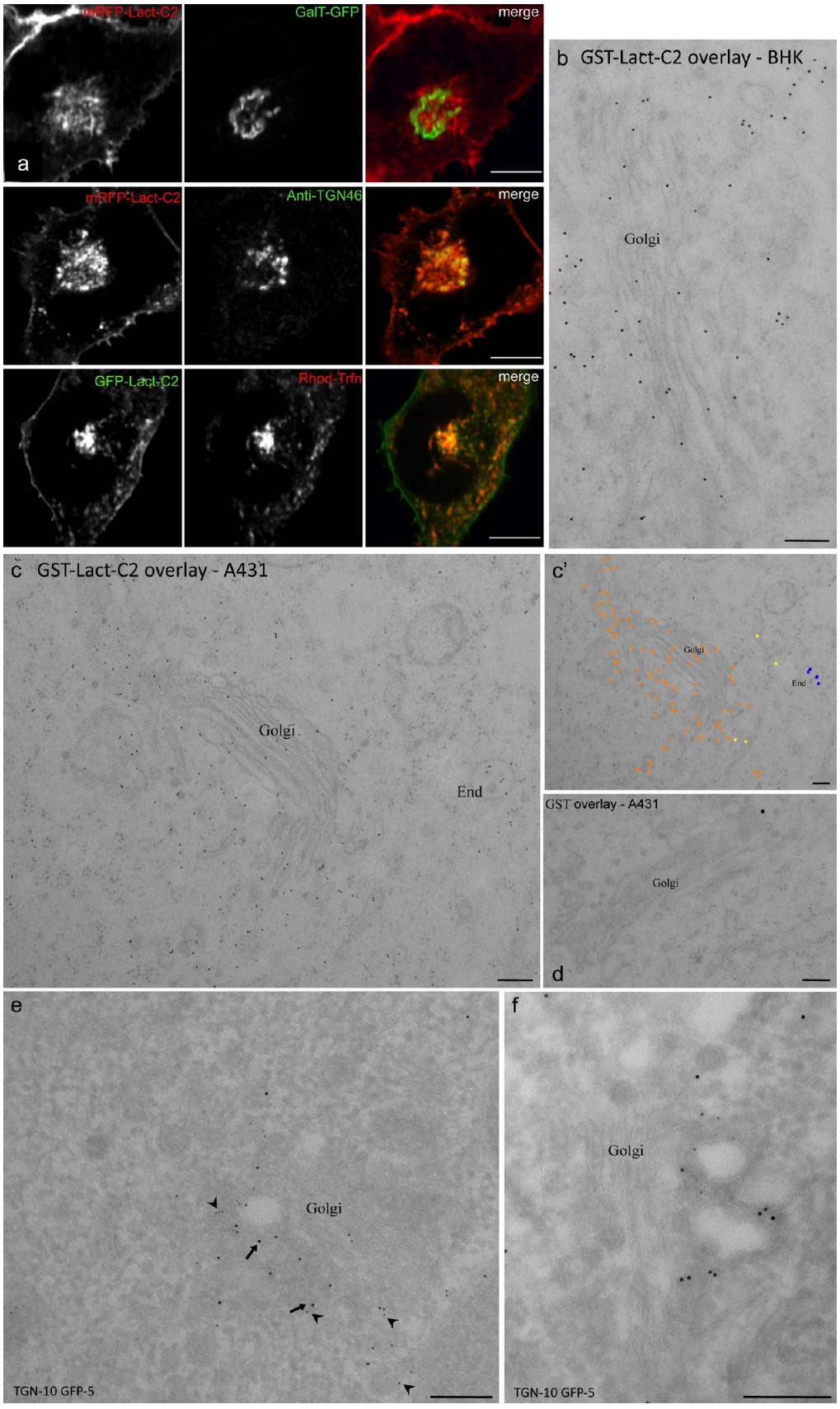

Figure 4. **Localization of PS to the Golgi complex and endosomes.** (a, top) HeLa cells transiently cotransfected with mRFP-Lact-C2 (left) and GalT-GFP (middle). (a, middle) HeLa cells transfected with mRFP-Lact-C2 were fixed, permeabilized, and immunostained for TGN46. (a, bottom) HeLa cells transiently transfected with GFP-Lact-C2 and incubated with rhodamine-transferrin for 30 min. (b–d) Cultured cells were processed using HPF/FS/LTE. Sections were

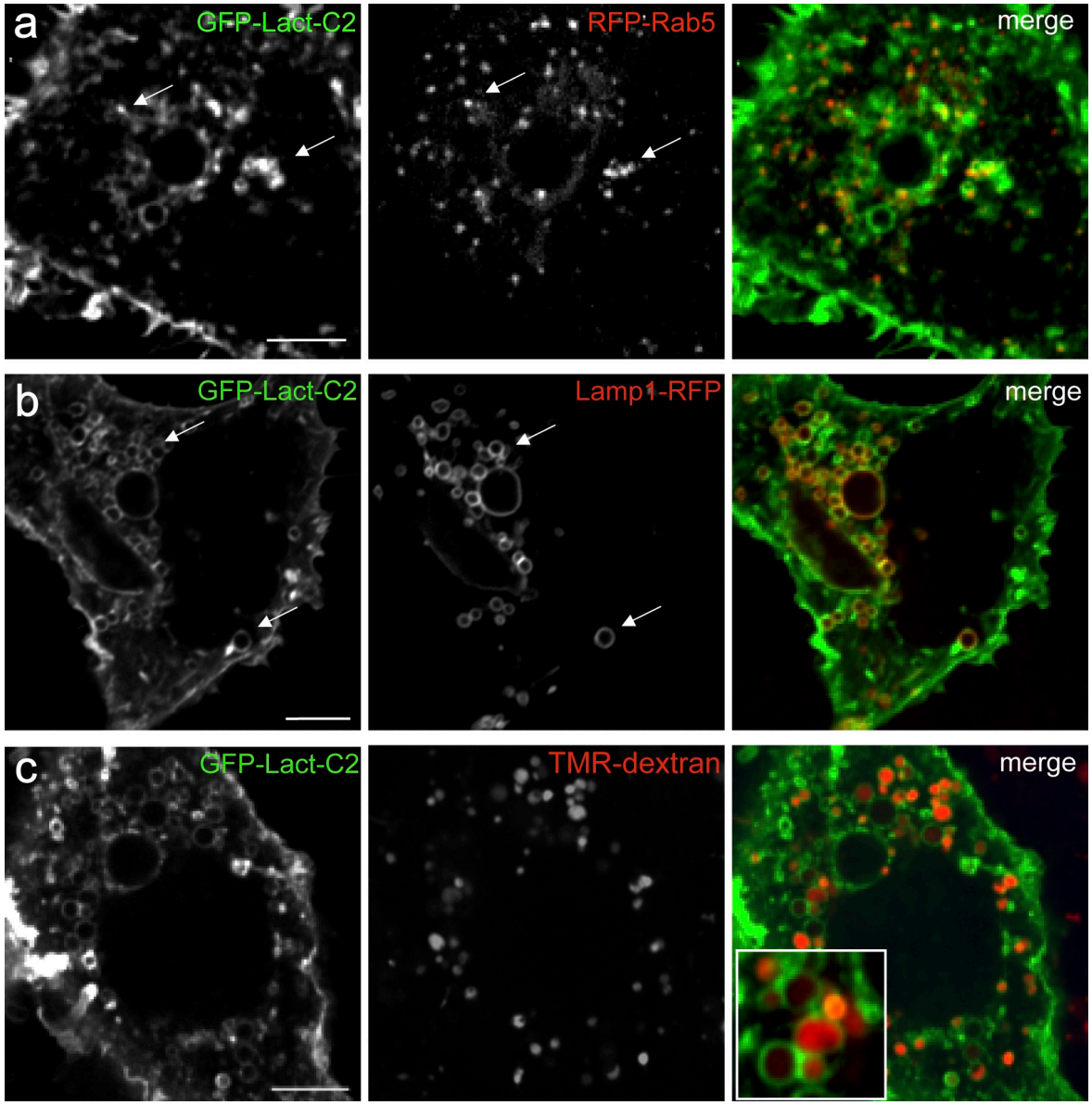

Figure 5. **Distribution of PS in the endocytic pathway.** A431 cells doubly transfected with GFP-Lact-C2 and RFP-Rab5 (a) or GFP-Lact-C2 and Lamp1-RFP (b), or transfected with GFP-Lact-C2, then incubated in the presence of tetramethylrhodamine (TMR) dextran for 16 h and chased for 1 h before visualization (c), as indicated. In a and b, arrows identify representative endosomal structures labeled by both markers. Inset shows enlarged views of the merged image. Bars, 5 µm.

content have been reported between the surface and lysosomal membranes. The PS content of the yeast vacuole, the equivalent to mammalian lysosomes, was estimated at <5%, markedly lower than that of the PM (~30%; Zinser et al., 1991). Whether this large difference also exists in mammalian cells, and the sidedness of PS in the endocytic pathway, have not been clearly established.

We therefore used Lact-C2 to analyze PS distribution in mammalian endosomes and lysosomes. In A431 cells, GFP-Lact-C2 overlapped extensively with the early endosomal markers RFP-Rab5 (Fig. 5) and 2x-FYVE-RFP, a reporter of phosphatidylinositol 3-phosphate (Fig. S1). Therefore, PS is present in both sorting and recycling endosomes. The compartments identified by Lamp1-RFP (Fig. 5), which correspond to late endosomes/lysosomes, were also extensively labeled by GFP-Lact-C2. To better discern the late stages of the endocytic pathway, we also analyzed the presence of PS in the subcompartment containing the

incubated with purified GST-Lact-C2 (b and c) or GST (d) and labeled as described in Materials and methods. c′ shows the image in c pseudocolored to highlight gold particles, color-coded to indicate specific compartments: orange, Golgi complex; blue, endosomes (End). (e and f) BHK cells transiently transfected with GFP-Lact-C2 and a TGN marker, GCC88-myc, fixed, frozen-sectioned, and double-labeled for TGN (arrows, large gold, 10 nm) and GFP (arrowheads, small gold, 5 nm). The expressed probe associates with membranes close to the Golgi but does not label the entire Golgi stack (e and f). In contrast, labeling with the overlaid probe is throughout the Golgi complex, including cisternae (b–c′). Bars: (a) 4 µm; (b–f) 200 nm.

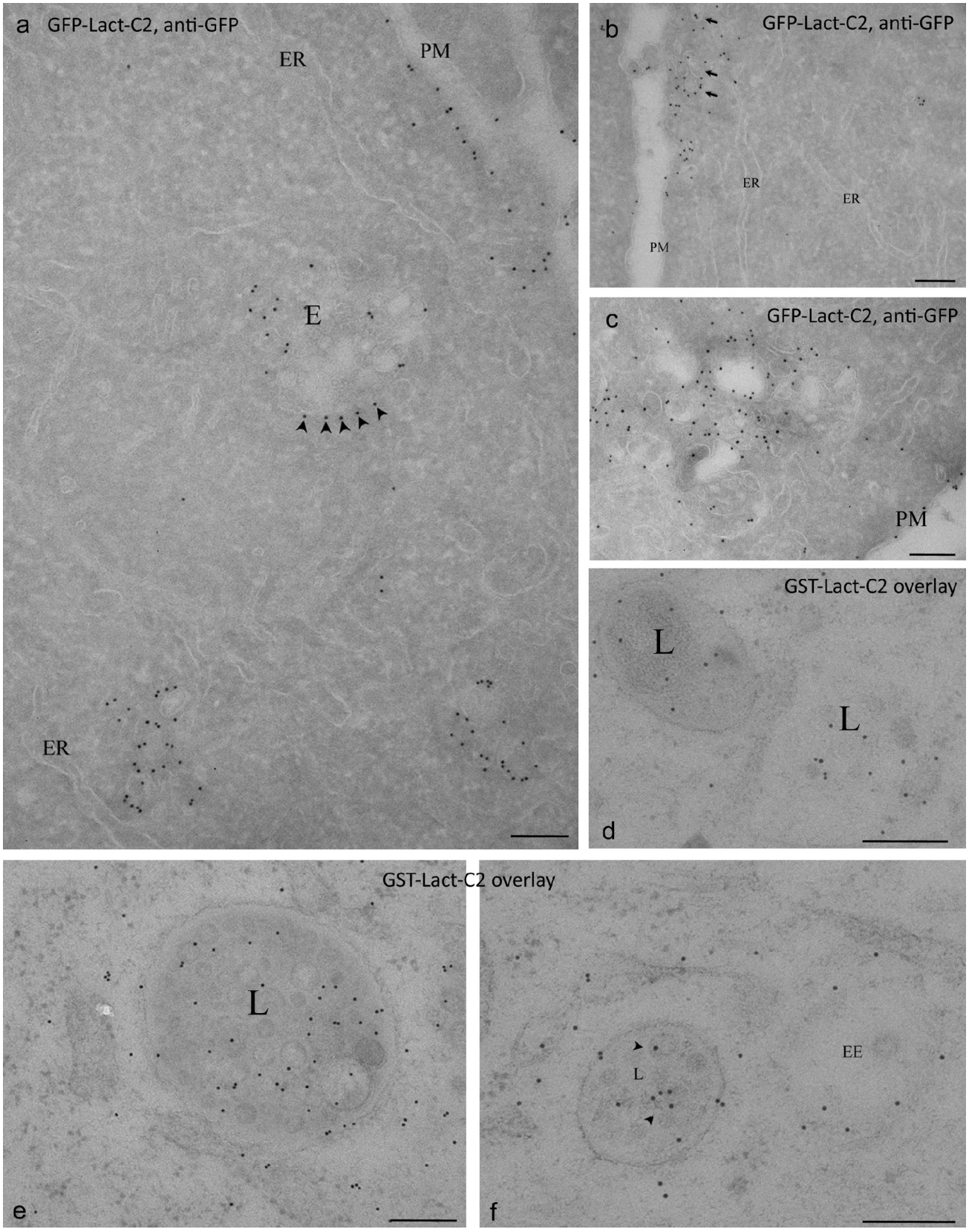

Figure 6. **Ultrastructural localization of PS in the endocytic pathway.** Cells transfected with GFP-Lact-C2 and GFP detected on frozen sections (a–c), or processed using HPF/FS/LTE and overlaid with purified GST-Lact-C2 (d–f). (a–c) The cytoplasmically expressed probe labels the PM but not the ER. Multivesicular endosomes (E) show strong labeling, particularly on the cytoplasmic aspect (e.g., arrowheads in a). Strong labeling is also evident in large vesicles close to the PM (arrows in B). (d–f) On-section labeling reveals labeling of internal membranes of MVB including putative late endosomes/lysosomes (L) and early endosomes (EE). Arrowheads indicate ILVs. Bars, 200 nm.

tetraspanin protein CD63 and analyzed selectively bona fide lysosomes using a pulse-chase protocol (see Materials and methods). As shown in Fig. S1, CD63-RFP, a marker of multivesicular late endosome/lysosomal compartments, overlapped extensively with GFP-Lact-C2 ($M_{red} = 0.75 \pm 0.01$; $P < 0.01$). Moreover, the limiting membrane of lysosomes preloaded with fluorescent dextran was also clearly stained by the PS probe (Fig. 5). Similar results were observed when A431 cells expressing GFP-Lact-C2 were stained with LysoTracker red, an acidotropic dye (Fig. S1). These results revealed that PS is detectable on the cytosolic leaflet of all the endocytic organelles, and suggest differences in PS handling between yeast and mammalian cells.

To gain further insight into the distribution of PS in the endocytic pathway, we used immunostaining of transfected GFP-Lact-C2 or the GST-Lact-C2 overlay approach using the HPF/FS/LTE, in combination with EM. Immunogold analysis of BHK cells expressing the cytoplasmic GFP-Lact-C2 showed labeling of early endosomes, recognized by their characteristic morphology (relatively electron-lucent, with a small number of intralumenal vesicles (ILVs) and a bilayered clathrin coat; Fig. 7) and of the limiting membrane of late endosomal multivesicular compartments (Fig. 6, a–c; and Fig. 7). The cytoplasmic probe should not recognize PS in the lumen of the endosome or within the interior of intralumenal vesicles (equivalent to the cytosol) of multivesicular bodies (MVBs), unless the latter acquired the probe before or during invagination. Remarkably, a strong labeling of ILVs in a subpopulation of late endosomes was observed on both frozen sections and with the HPF/FS/LTE technique. The latter method, which avoids fixation, allowed us to precisely localize the probe labeling to a distinct subpopulation of ILVs in some late endosomes, which suggests that these vesicles were generated after expression of the probe within the cytoplasm, and that interaction with PS on the cytoplasmic face of the endosome followed by ILV formation carried the probe into the interior of the endosome. A striking heterogeneity in ILV labeling was apparent with this technique, with some late endosomes showing only labeling of the limiting membrane and others showing strong internal labeling (the mean percentage internal labeling was 37.8 ± 7.7%, but with variation from 0 to 79%). The post-sectioning overlay technique not only replicated the labeling of the limiting membrane of early and late endosomes in mouse liver, BHK cells (not depicted), and A431 cells (Fig. 6, d–f), but clearly demonstrated the presence of PS in the membrane of late endosomal luminal vesicles with consistently high labeling in the interior (65.5 ± 2.7%).

Delivery of PS to the PM

PS is synthesized in the ER and seemingly delivered to the PM by vesicular traffic. However, its concentration in the membrane increases and its sidedness is altered, with virtually all the PS found on the cytosolic aspect of the PM. To analyze where such changes occur, we followed the fate of PS dynamically along the secretory pathway. To this end, we expressed a temperature-sensitive form of vesicular stomatitis virus G, VSVG-ts045, tagged with GFP. The labeled protein enabled us to monitor the movement of biosynthetic cargo through the cell in a manner that can be controlled by altering the temperature (Presley et al., 1997). When cells expressing VSVG-ts045 are grown at 40°C, the protein is retained in the ER in a misfolded state (de Silva et al., 1993), but folds and is exported when the cells are incubated at a lower, permissive temperature. For our studies, VSVG-GFP was transiently cotransfected with mRFP-Lact-C2 into COS7 cells and grown overnight at 40°C. As shown in Fig. 8 a, when cells were maintained at 40°C, VSVG-GFP was found to remain associated with the ER. Under these conditions, no significant overlap of VSVG-GFP with RFP-Lact-C2 was observed, which is consistent with the earlier conclusion that little PS is exposed on the cytosolic leaflet of the ER. Incubation of cells at 20°C led to proper folding and exit of VSVG-GFP from the ER. However, at this temperature, transport out of the Golgi is blocked. After 60 min at 20°C, a large portion of the VSVG-GFP migrated to the Golgi complex (Fig. 8 b). Remarkably, very little colocalization was found at this stage between VSVG-GFP and mRFP-Lact-C2. Under these conditions, mRFP-Lact-C2 colocalized with TGN46 (Fig. 8 b), which suggests that when arrested for 1 h at 20°C, cargo such as VSVG-GFP accumulates in the Golgi cisternae, but does not reach the TGN. Accordingly, when cells expressing VSVG-GFP and grown overnight at 40°C were shifted to 20°C for 60 min and immediately fixed and immunostained with anti-TGN46 antibodies, the clustered VSVG-GFP puncta were adjacent to, but not overlapping, structures identified as TGN (Fig. 8 d).

Transferring cells that had been arrested at 20°C to 37°C facilitated the formation of secretory vesicles and export of material from the Golgi. This maneuver promoted the appearance of more peripheral vesicles that contained both VSVG-GFP and RFP-Lact-C2 (Fig. 8 c). Together with our ultrastructural studies, these findings imply that substantial PS becomes exposed on the cytosolic leaflet of vesicles after they leave the Golgi stacks, likely at the TGN stage.

Ca^{2+}-induced PS externalization and apoptosis

Increases in cytosolic Ca^{2+} induce the scrambling of PM aminophospholipids, leading to the appearance of PS in the exofacial leaflet. Similar scrambling of PM lipids also accompanies apoptosis. However, little is known about the fate of PS in endomembranes under these circumstances. We used the approaches described in the preceding section to analyze PS distribution in cells treated with ionophores (to elevate cytosolic Ca^{2+}) or with antibody to FAS (to initiate apoptosis).

In resting HeLa cells, where PS is detectable in the PM inner leaflet using GFP-Lact-C2, only negligible amounts of PS are exposed on the outer surface. The addition of ionomycin in the presence of Ca^{2+} induced lipid scrambling. This became readily apparent upon addition of annexin V, an extracellularly added PS ligand that fails to interact with intact cells but binds avidly to the outer surface of ionophore-treated cells (Fig. 9 a). Exofacial binding of annexin V was associated with loss of GFP-Lact-C2 from the inner surface, which is consistent with net displacement of PS across the plasmalemmal bilayer. The loss of PM probe is associated with increased labeling of endomembranes. It is unclear whether this signals increased PS

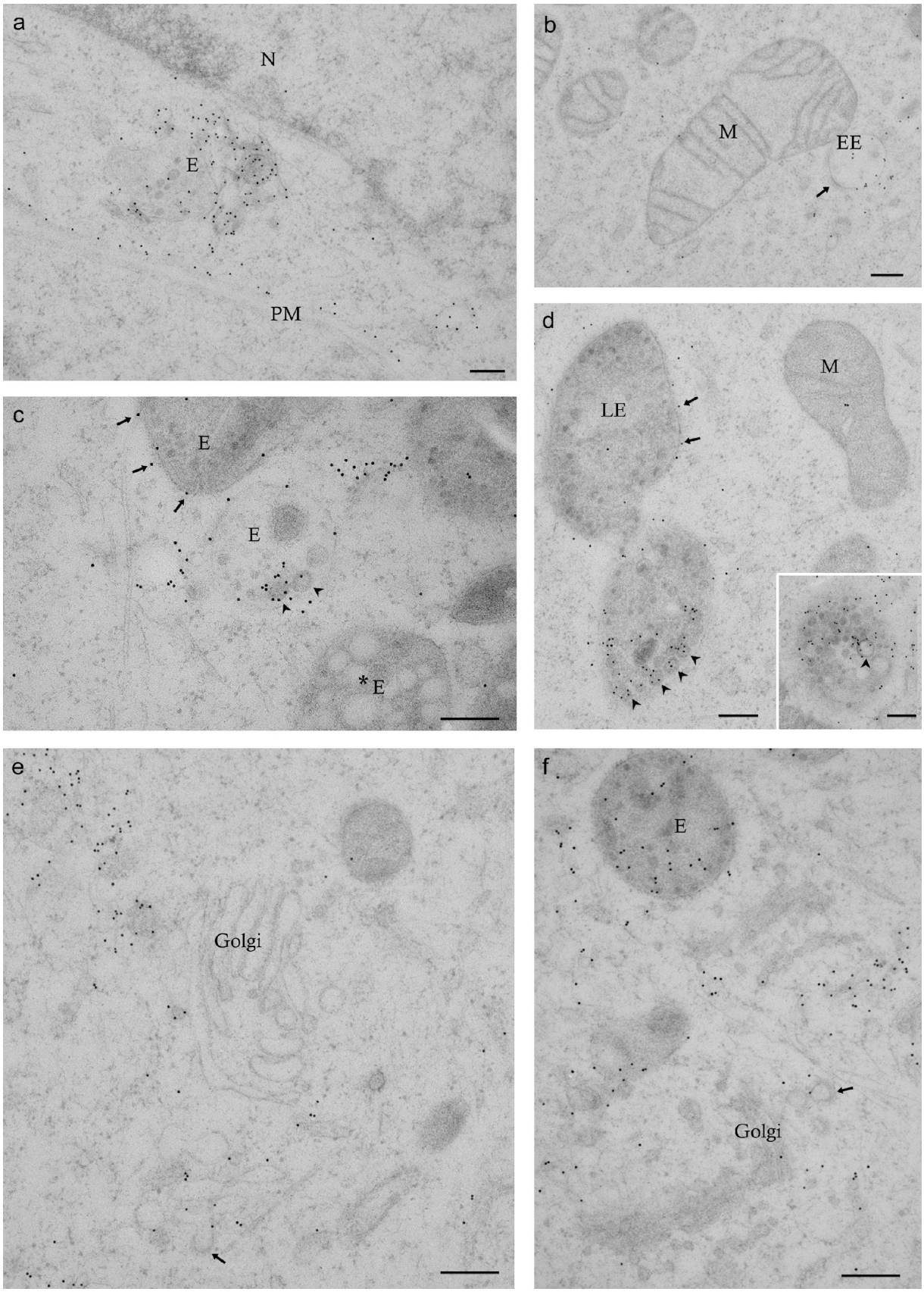

Figure 7. **Ultrastructural localization of the cytoplasmically expressed GFP-C2 probe; HPF-FS method.** BHK cells expressing GFP-Lact-C2. Cells were high-pressure frozen, freeze-substituted, and embedded in UV-polymerized Lowicryl at low temperature. Sections were immunogold-labeled for GFP. (a) Low-magnification overview showing specificity of labeling (top cell transfected, bottom cell untransfected). Note the high labeling on the PM and on

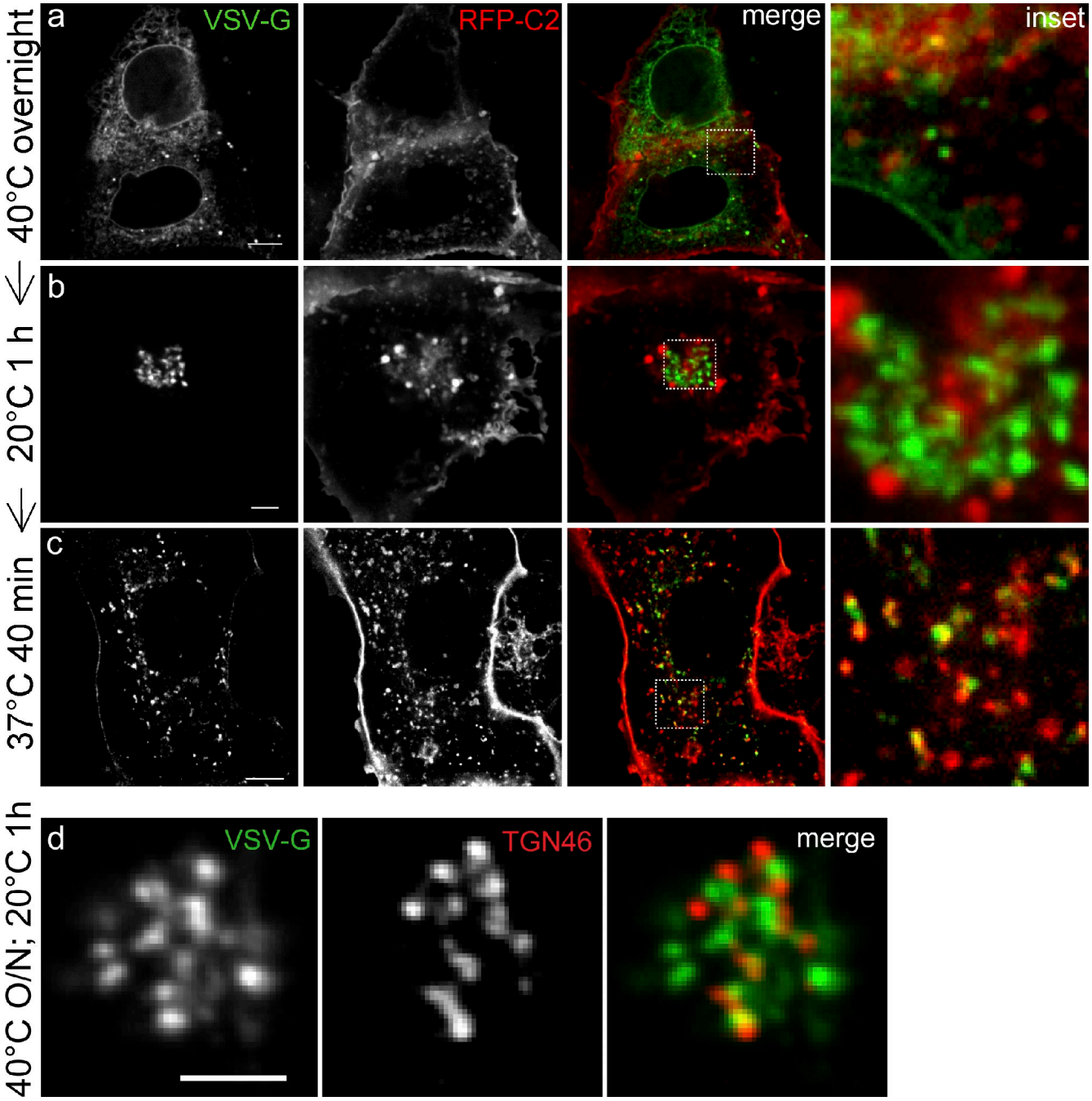

Figure 8. **PS becomes cytosolically exposed during progression through the secretory pathway.** COS7 were cells double-transfected with VSVG-GFP and mRFP-Lact-C2 (a–c), then incubated as indicated to label the ER (40°C overnight), the Golgi complex (20°C for 1 h after 40°C overnight), and post-Golgi compartments (37°C for 40 min, after 40°C overnight followed by 1 h at 20°C). Insets show enlargement of indicated merged image. Cells expressing VSVG-GFP (d) were grown overnight at 40°C, then shifted to 20°C for 1 h, fixed, and immunostained for TGN46. Insets show enlarged views of the boxed region in the merged image. Bars, 5 μm.

multivesicular endosomes (E) and the absence of labeling of the nuclear envelope. (b–f) Gallery of representative images showing labeling of endosomes but low labeling of mitochondria (M) and Golgi cisternae (G). (b) A putative early endosome (EE), recognizable by the bilayered clathrin patch (arrow), shows significant labeling. (c–e) Individual multivesicular endosomes show distinct labeling patterns including cytoplasmic staining (c and d, arrows), predominantly internal labeling (f), a mixture of the two, or unlabeled (c, asterisk). Note the striking labeling of a specific subpopulation of internal membranes in c, d, and the inset (arrowheads). (e and f) Golgi cisternae show negligible labeling, but vesicles and tubules close to the Golgi, putative TGN elements, including clathrin-coated buds (arrows), show significant labeling. Bars, 200 nm.

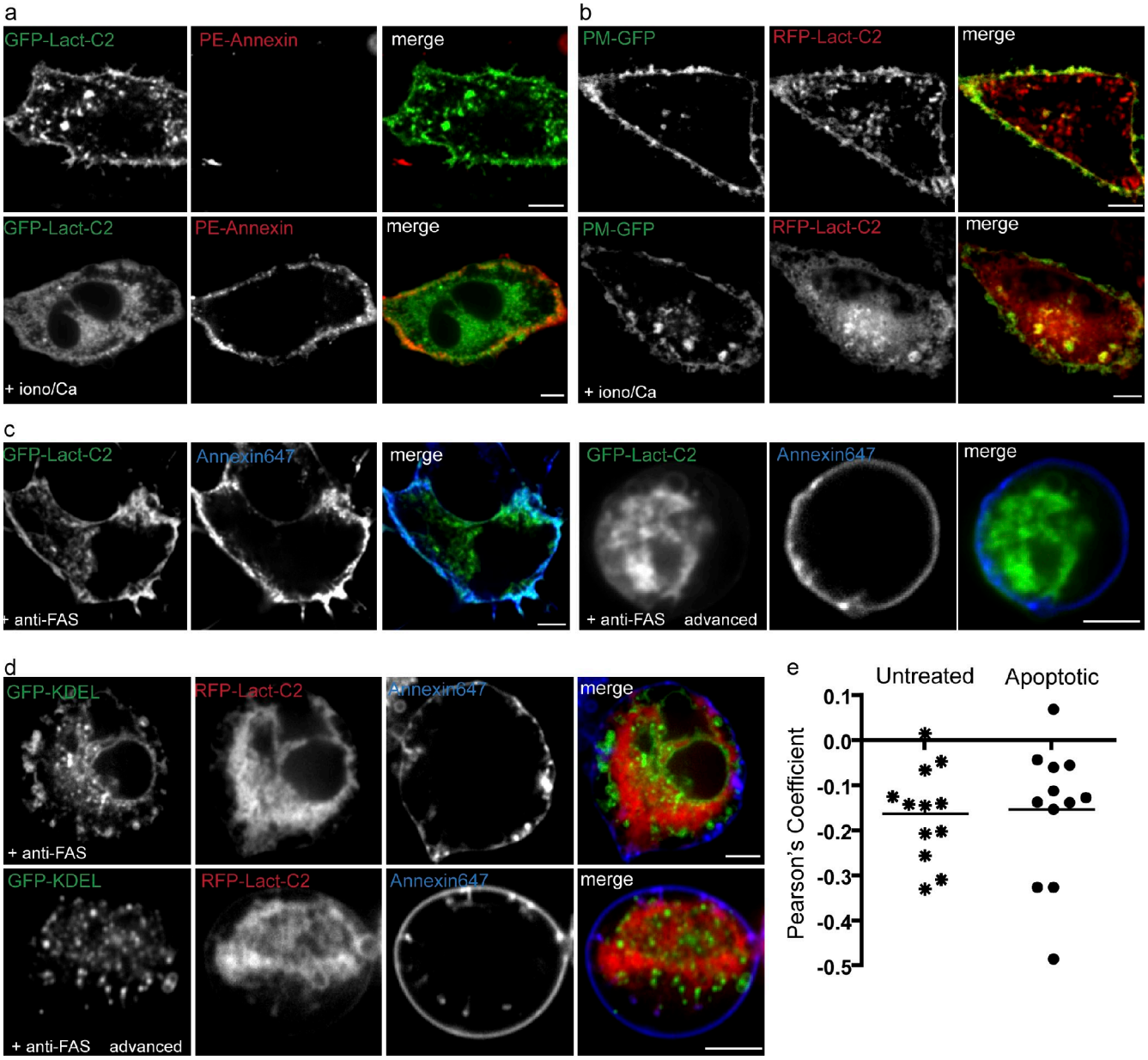

Figure 9. **Distribution of PS following elevation of cytosolic Ca^{2+} and induction of apoptosis.** (a and b) HeLa cells transfected with GFP-Lact-C2 (a) were incubated with phosphatidylethanolamine-conjugated annexin V, or GFP-Lact-C2 and PM-RFP (b), and imaged before (top) or 10 min after treatment with 10 µM ionomycin in the presence of 2.5 mM Ca^{2+} (bottom). (c and d) Cells were transfected with GFP-Lact-C2 (c) or cotransfected with RFP-Lact-C2 and GFP-KDEL (d). Cells were exposed to anti-FAS IgM (1.5 µg/ml) and images were acquired after 4 h. Apoptotic cells were identified using Alexa Fluor 647–conjugated annexin V. Cells that had undergone rounding are deemed to be in a more advanced state of apoptosis. Images in a and d are representative of three experiments of each type. Bars, 10 µm. (e) Pearson's correlation coefficients calculated to assess the colocalization of RFP-Lact-C2 and GFP-KDEL. Values obtained separately for 12 untreated (*) and 12 apoptotic cells (●) are plotted; the mean for each dataset is indicated by the horizontal line.

exposure of internal organelles or merely reflects the increased availability of the probe as a result of its release from the surface membrane. Accelerated endocytosis is unlikely to account for the observed increase in endomembrane staining, as the generic membrane marker (PM)-RFP redistributed only modestly (Fig. 9 b).

Though rapid and effective, the scrambling of lipids induced by elevated Ca^{2+} is not a normal physiological event. We therefore also studied PS in cells where apoptosis was triggered by cross-linking FAS using antibodies. When exposed to the anti-FAS receptor IgM, 40–50% of the HeLa cells underwent apoptosis within 4 h, as evinced by DNA condensation. A similar fraction of the cells bound annexin V, verifying the occurrence of PS scrambling. At this stage, some of the annexin V–positive cells maintain near-normal morphology, whereas others had become rounded, which we interpret as having entered a more advanced stage of apoptosis (Fig. 9 c). Although the changes in GFP-Lact-C2 distribution were minor in cells that preserved their shape, the PS probe detached from the PM and associated with endomembranes in the rounded cells, resembling the effects of Ca^{2+} elevation (Fig. 9 c). We next considered whether in apoptotic cells PS had become exposed on the cytosolic aspect of the ER membrane. To this end, cells cotransfected

with GFP-KDEL and RFP-Lact-C2 were treated with anti-FAS IgM (Fig. 9 d). In cells at the more advanced stage of apoptotic progression, the ER appeared distorted and fragmented. However, even in these instances, the RFP-Lact-C2 probe failed to colocalize with the ER (Fig. 9 e; the colocalization coefficient was insignificant: -0.154 ± 0.048; mean ± SEM, $n = 12$). Thus, while undergoing major rearrangements in the plasmalemma, we found no evidence that the distribution of PS was altered in the ER. Qualitatively similar observations were made with HeLa cells subjected to anti-FAS antibody treatment and analyzed by overlay EM after fast freezing (unpublished data).

Discussion

The advent of stereospecific probes has made it possible to detect PS in intact or sectioned cells, providing a useful complement to other lipidomic techniques. In this manuscript, we extended the analysis by fluorescence microscopy of discoidin C2 domain probes and introduced their application to EM. Immunogold labeling of genetically encoded, endogenously expressed C2 domains, in combination with the overlay of sectioned samples with recombinant C2 domain, offered new insights into the distribution of PS at the ultrastructural level. In addition, we demonstrated that a simple processing scheme involving fast-freezing, FS, and LTE provides excellent lipid retention and ultrastructural preservation and is compatible with immunolabeling. The method used involves a relatively rapid FS protocol and only staining with uranyl acetate (avoiding osmium and other stains), with some resulting loss of membrane contrast. Nevertheless, we believe that the advantages of a method that avoids primary fixation and is compatible with lipid and protein localization, while retaining GFP fluorescence (Nixon et al., 2009), outweigh this disadvantage. Indeed, comparison of frozen sections and the HPF/FS/LTE sections demonstrated the difficulties that can be encountered in labeling Tokuyasu sections with lipid probes. Although PM labeling was negligible, labeling of multivesicular endosomes remained high, thus biasing the labeling toward this compartment. The application of lipid-binding probes "on section" under nonperturbing conditions where lipids are retained in their native distribution represents a great advance over existing methods.

Establishment of subcellular PS distribution and asymmetry

PS is synthesized in the ER and catabolized primarily in the mitochondria. It is therefore remarkable that PS is virtually undetectable in these compartments when using the cytosolically expressed Lact-C2 probe. Although PS is continuously exported from the ER through the secretory pathway, its removal accounts only in part for the inability of the cytosolic C2 domains to detect it because positive labeling was obtained when sectioned samples were overlaid with Lact-C2. Instead, we interpret the results to mean that a large fraction of the PS of the ER resides in the lumenal monolayer. This appears to conflict with the notion that phospholipids synthesized on the lumenal aspect are randomly "scrambled" across the bilayer to minimize induction of curvature and to allow membrane expansion (Bell et al., 1981; Bishop and Bell, 1985; Herrmann et al., 1990). However, our interpretation is consistent with direct measurements of PS distribution based on accessibility to phospholipases (Higgins and Dawson, 1977).

Like the ER, the Golgi cisternae showed little labeling with the cytosolic PS probe, which was instead distinctly associated with membranes of the TGN. It is likely that the PS that is predominantly lumenal in earlier secretory compartments is flipped to the cytosolic leaflet at this station. Accordingly, the type IV P-type ATPases that are thought to mediate aminophospholipid translocation across the bilayer are uniquely accumulated in the Golgi complex. In yeast, where the most detailed information is available, five distinct isoforms of these putative flippases reside primarily in late- and post-Golgi membranes (Muthusamy et al., 2009). A byproduct of the uncompensated flipping of aminophospholipids is the generation of membrane curvature (Liu et al., 2008; Graham and Kozlov, 2010). If properly harnessed by additional protein machinery, these local deformations could assist in vesicle formation, which may be an integral part of the secretory process.

It is noteworthy that, in cells incubated at 20°C, recently folded VSVG-GFP accumulated in the Golgi complex, yet did not colocalize with the TGN marker TGN46. Thus, traffic was arrested before the delivery of cargo to the TGN exit sites. It is tempting to speculate that failure of the PS flippases to operate normally at 20°C may have contributed to the traffic arrest.

PS topology and distribution in apoptotic cells

The human body has been estimated to recycle 10^6 cells/s (Henson and Hume, 2006); the unwanted cells are effectively engulfed by phagocytes. Externalization of plasmalemmal PS provides the "eat me" signal that identifies cells targeted for degradation. The preexisting PS asymmetry is lost in apoptotic cells upon activation of phospholipid scramblase. The scramblase is also activated acutely by elevation of cytosolic Ca^{2+}, a process of vital importance in blood coagulation. Although the appearance of exofacial PS has been well documented, the possible occurrence of associated changes in intracellular PS distribution had not been explored.

As expected, we found that PS was rapidly externalized by HeLa cells treated with the Ca^{2+} ionophore, ionomycin. Under these conditions, a substantial fraction of the PS-sensing probe was released from the inner aspect of the PM, associating instead with endomembranes. A similar redistribution was noted in cells undergoing apoptosis, particularly those at advanced stages of the process. Despite the marked increase in endomembrane labeling, the Lact-C2 probe failed to associate significantly with the ER. This suggests that the mechanisms that retain PS in the luminal leaflet of the ER remain functional in apoptotic cells.

It is unclear if the increased labeling of endomembranes seen in Ca^{2+}-treated or apoptotic cells reflects elevated concentrations of PS or mostly increased availability of the Lact-C2 probe, which is partially released from the plasmalemmal inner surface. Nevertheless, the data imply that endogenous PS-associated molecules, such as those containing canonical C2 domains or γ-carboxy glutamic acid, will undergo a similar fate, detaching in part from the membrane to attach elsewhere inside the cell.

Is PS enriched in membrane microdomains?

The long-standing fluid mosaic model of biological membranes has been challenged in recent years by the observation that membrane proteins and lipids are differentially sensitive to extraction by nonionic detergents. This led to the proposal that the membrane is instead segregated into microdomains, a notion that has been confirmed by a variety of physical and biochemical approaches (Lingwood and Simons, 2010). We used high-resolution spatial mapping to analyze whether PS was distributed inhomogeneously in the PM. Point-pattern analysis of immunogold-labeled membranes revealed that PS was concentrated in nanoclusters of 11 nm.

Lipid rafts represent a well-studied, but still enigmatic, surface microdomain (Simons and Gerl, 2010). Morphologically identifiable caveolae represent one specific type of stabilized raft microdomain. As illustrated in Figs. 1 and S3, significant labeling of PS was associated with caveolae. Although the high degree of curvature of caveolae makes quantitation of enrichment in these structures compared with the bulk membrane difficult, cells with low expression of the C2 domain showed distinct accumulation of this PS probe in regions enriched in caveolae. What might be the mechanism for this enrichment? A caveolin peptide has been shown to induce redistribution of PS in a liposome-based model system (Wanaski et al., 2003), raising the possibility that caveolin could drive the formation of domains enriched in PS. Interestingly, all four members of the cavin coat protein family have been shown to bind PS in vitro (Bastiani and Parton, 2010). As cavins are recruited to surface caveolae by caveolin but are not recruited to caveolin in transit through the Golgi complex (Bastiani et al., 2009), the stabilization of caveolae by cavins may rely on combined low-affinity interactions between the cavin complex and both PS and caveolin, with neither interaction on its own sufficing to recruit cavin to the surface. Alternatively, the concentration of cavins in caveolae could have an active role in bringing together PS nanoclusters in caveolae. Lastly, lipid-based sorting could also potentially lead to enrichment of PS in caveolae. A subpopulation of PS molecules may partition preferentially in the sphingolipid and cholesterol-enriched liquid-ordered domain and become part of the stabilized rafts present in caveolae.

Fate of PS in the endocytic pathway

Because of its prevalence in the PM, it is not surprising that PS is delivered to early endosomes via a variety of internalization mechanisms. Accordingly, we found clear association of the Lact-C2 probes with sorting and recycling endosomes, in good agreement with subcellular fractionation studies (Gagescu et al., 2000). The concomitant enrichment of cholesterol, sphingomyelin, and PS in recycling endosomes (Gagescu et al., 2000) is consistent with the incorporation of PS into liquid-ordered structures delivered to endosomes by internalization of caveolae or related microdomains.

Earlier biochemical studies indicated that the transition from early to late endosomes/lysosomes is associated with a decrease in PS, cholesterol, and sphingomyelin, which is compensated in part by the appearance of the atypical lipid bis(monoacylglycerol)phosphate (Kobayashi et al., 2002). Selective recycling of membrane raft components to the PM and/or retrograde transport to the Golgi may help account for the decrease in cholesterol, sphingolipids, and PS in the late compartments of the endocytic pathway and their enrichment in the PM. Such sorting may occur by outward budding of the limiting membrane of endosomes, but also via formation of internal vesicles. Fractionation of MVB revealed the existence of two separate components, one of which was endowed with both PS and CD63, a stable constituent of late endosomes/lysosomes. Because a fraction of the lumenal vesicles of MVB undergo back-fusion with the limiting membrane, those containing CD63 may serve to redirect PS to other compartments of the endocytic or secretory pathway.

Our studies confirm the presence of PS in intralumenal vesicles of MVB and are also compatible with studies of PS in exosomes (Laulagnier et al., 2004; Trajkovic et al., 2008), which arise from secretion of the contents of MVB. Interestingly, exosomes not only contain elevated PS, but are also rich in cholesterol and ceramide (Wubbolts et al., 2003; Laulagnier et al., 2004; Trajkovic et al., 2008) compared with total cellular membranes. In oligodendrocytes, the formation of exosomes is independent of the ESCRT machinery and instead appears to rely upon the generation of ceramide from sphingomyelin via neutral sphingomyelinase 2. These observations suggest a mechanism whereby PS associated with cholesterol may be selectively redirected to a unique subpopulation of intralumenal vesicles. A separate, PI3P-enriched subpopulation is likely generated via the ESCRT pathway (Raiborg and Stenmark, 2009; Wollert and Hurley, 2010). Consistent with the presence of distinct classes of ILVs in the endosomal system was the observation that the cytoplasmically expressed probe labeled a specific subpopulation of ILVs within some late endosomes, whereas morphologically identical late endosomes in the same cells only showed labeling of the limiting membrane. This presumably reflects the recognition of PS on the limiting membrane and then ILV formation, and suggests intriguing differences in the dynamics of ILV formation among individual late endosomes within the cellular late endosomal population.

Concluding remarks

Together with earlier findings, our results highlight a remarkable cosegregation of PS with cholesterol and sphingolipids in the various cellular subcompartments; the highest concentration of these lipids is found in the plasmalemma and in early endocytic compartments, whereas the ER is comparatively devoid of all three. Moreover, the enrichment of cholesterol and sphingolipids along the secretory pathway occurs in the late stages of the Golgi complex, where PS became apparent in the cytosolic leaflet. The mechanistic relationship between these events remains to be defined, but it is clear that dynamic techniques that preserve organellar integrity, such as those used in the present work, will contribute to our understanding of the establishment of lipid inhomogeneity and transmembrane topology.

Materials and methods

Reagents

Cholera toxin B conjugated to Alexa Fluor 488, LysoTracker Red, tetramethylrhodamine transferrin, and tetramethylrhodamine dextran were purchased from Invitrogen. Anti-TGN46 antibody was purchased from AbD Serotec.

Plasmids

The GFP-KDEL was constructed by adding the nucleotides encoding the amino acids KDEL (5′-AAAGATGAGTTG-3′) to the C-terminal end of the GFP open reading frame. The clathrin light chain was cloned into the EcoRI and SalI sites of the pEYFP-C1. The GFP-Lact-C2 and mRFP-Lact-C2 were constructed first by PCR amplifying the bovine C2 domain of Lactadherin and subsequently cloned into the pEGFP-C1 and mRFP-Lact-C2 vectors, respectively, using the BglII and EcoRI sites (Touret et al., 2005; Yeung et al., 2008). CD63-mCherry was a gift from W. Trimble (Hospital for Sick Children, Toronto, Ontario, Canada). GalT-GFP was provided by E. Rodriguez Boulan (Weill Cornell Medical College, New York, NY). The 2xFYVE-RFP was provided by L. Cantley (Harvard University, Cambridge, MA), and the GFP-p40-PX by M.B. Yaffe (Massachusetts Institute of Technology, Cambridge, MA). The PH domain of PLCδ was provided by T. Balla (National Institutes of Health, Bethesda, MD) and the VSVG-GFP ts045 construct was provided by J. Lippincott-Schwartz (National Institutes of Health). Sec61α-GFP (Greenfield and High, 1999), RFP-Rab5 (Vonderheit and Helenius, 2005), and Lamp1-RFP (Sherer et al., 2003) were described earlier and mito-RFP was obtained from Invitrogen. The TGN marker GCC88-myc was provided by J. Stow (Institute for Molecular Bioscience, the University of Queensland, Brisbane 4072 QLD, Australia) and described previously (Luke et al., 2003).

Cell culture and transfections

A431, HeLa, and COS7 cells from the American Type Culture Collection (ATCC) were maintained in DME + 10% fetal bovine serum (ATCC). Transient transfection of plasmids was performed using FuGene6 (Roche) according to the manufacturer's instructions.

3T3-L1 fibroblasts (ATCC) were maintained in DME supplemented with 10% (vol/vol) FCS (Hyclone; Invitrogen) and 2 mM L-glutamine (Invitrogen). 3T3-L1 fibroblasts were induced to differentiate by addition of 4 µg/ml insulin, 0.25 mM dexamethasone, 100 ng/ml biotin, and 0.5 mM isobutyl-methylxanthine to confluent cells for 72 h. After 72 h, the medium was replaced with fresh DME containing 10% FCS and 4 µg/ml insulin for a further 72 h. Differentiated cells were fed with FCS/DME every 48 h and used between days 6 and 12 after differentiation (Martin et al., 2005).

A431 and BHK-21 cells were maintained in DME supplemented with 10% (vol/vol) FCS and 2 mM L-glutamine. Transfection of BHK-21 cells was performed using Lipofectamine 2000 (Invitrogen) according to the manufacturer's instructions. Transfection was overnight in all experiments, except for the double transfections of GCC88-myc plus GFP-Lact-C2 (7 h) because of the altered Golgi morphology in some of the cells expressing high levels of GFP-Lact-C2.

Protein purification and lipid-protein overlay assay

The pGEX-Lact-C2 plasmid was transformed into *Escherichia coli* BL21 (DE3; EMD), and protein expression was induced by addition of 0.5 mM IPTG to exponential-phase bacteria. After 3 h at 30°C, the bacteria were harvested and lysed with B-PER reagent (Thermo Fisher Scientific), affinity-purified using glutathione-Sepharose (GE Healthcare), and eluted with glutathione-containing buffers.

Phospholipid-binding assays were performed essentially as described previously (Dowler et al., 2002) using lipid strips supplied by Echelon Biosciences Inc. Nitrocellulose membranes were spotted with 100 pmoles of the specified lipid. Blots were blocked with TBS containing 3% (wt/vol) fatty acid-free bovine albumin. Purified GST-Lact-C2 fusion proteins were incubated at 4°C for 12 h with the immobilized phospholipids in TBS containing 3% albumin. Blots were washed with TBS containing 0.5% Tween 20 and incubated for 1 h at room temperature with anti-GST primary antibody (1:5,000) followed by an anti–mouse secondary antibody (1:5,000) coupled to horseradish peroxidase. After washing with TBS containing 0.5% Tween 20, phospholipid binding was determined by enhanced chemiluminescence (GE Healthcare).

Fluorescence microscopy

Individual coverslips with transfected cells were transferred to a Chamlide CMB holder, medium was replaced with Hepes-buffered RPMI, and the chamber was placed in a microscope stage heater set to 37°C. Fluorescence images were acquired using spinning-disk confocal microscopy. The spinning-disk confocal systems (Quorum Technologies) used in our laboratory are based on an Axiovert 200M microscope (Carl Zeiss) with 63× (NA 1.4) or 100× (NA 1.45) oil immersion objective lenses, equipped with diode-pumped solid-state lasers (440, 491, 561, 638, and 655 nm; Spectral Applied Research) and a motorized XY stage (Applied Scientific Instrumentation). Images were acquired using a back-thinned, electron-multiplied (model C9100-13 ImagEM; Hamamatsu Photonics) or conventional cooled charge-coupled device (model C4742-95-12ER; Hamamatsu Photonics) cameras controlled by Volocity software 4.1.1 or 5.2.1 (PerkinElmer). Live cell imaging was performed at 37°C in Hepes-buffered RPMI. Total internal reflection fluorescence microscopy was performed using an Olympus system equipped with Argon (488 nm) and HeNe-G (543 nm) lasers.

Ionomycin and anti–FAS-induced apoptosis

Ionomycin was used to elevate cytosolic calcium and thereby induce lipid scrambling. Cells were bathed in synthetic medium consisting of 150 mM NaCl, 5 mM KCl, 1 mM $MgCl_2$, 100 µM EGTA, 2.5 mM $CaCl_2$, 20 mM Hepes, pH 7.4, and 4.5 g/liter glucose, and the reaction was initiated by addition of 10 µM ionomycin. Exofacial exposure of PS was monitored using either R-phycoerythrin- or Alexa Fluor 647–conjugated annexin V (Invitrogen). Images were acquired 5–10 min after the addition of the ionophore.

Apoptosis was induced by the addition of anti-FAS IgM (obtained from Beckman Coulter) to a final concentration of 1.5 µg/ml. Cells were imaged by spinning-disc confocal microscopy 3.5–4 h after addition of the cross-linking antibody. Apoptotic cells were identified using either fluorescent dye-conjugated annexin V to detect externalized PS or DAPI to visualize condensed DNA.

VSVG-GFP trafficking assay

COS7 cells were seeded on glass coverslips in a 12-well plate. The following day, cells were transfected with VSVG-GFP ts045 and, where specified, with mRFP-Lact-C2 as well, then incubated overnight at 40°C. At the indicated times, cells were fixed in 4% paraformaldehyde/PBS. To allow VSVG-GFP to exit from the ER and accumulate in the Golgi, the cells were incubated at 20°C in Hepes-buffered RPMI (Wisent Bioproducts). To visualize secretory vesicles in transit to the PM, after the 20°C block, the cells were transferred to medium prewarmed to 37°C. For TGN46 staining, cells were permeabilized with 0.1% Triton X-100/PBS and stained using anti-TGN46 (AbD Serotec), followed by Cy3-conjugated anti–sheep antibody.

Electron microscopy

Samples were high-pressure frozen, processed for FS, and embedded in UV-polymerized Lowicryl HM20 at low temperature essentially as described by Nixon et al. (2009). In brief, samples were placed into membrane carriers (zebrafish in 200 µm; cells and liver in 100 µm) in appropriate media (0.7% low melting temperature agarose in E3 for zebrafish, in growth medium for cells, and in low glucose-DME without FCS for liver) and kept at 37°C on a heating pad before they were high-pressure frozen using the EM PACT2 HPF (Leica). A431 cells were grown on sapphire discs that were placed into 100-µm membranes for freezing. Frozen samples then underwent FS in the EM AFS2 (Leica) with 0.2% uranyl acetate as the only staining/fixation agent. This was followed by infiltration with dilutions of Lowicryl HM20 resin in acetone (50% resin, 75% resin, and three changes of 100% resin) at −50°C and polymerization under UV light for 48 h at −50°C. The samples then warmed to 20°C and polymerized for a further 48 h (Nixon et al., 2009; Schieber et al., 2010).

Samples of adherent cells processed for Tokuyasu embedding were first washed with PBS, then scraped gently in 1% gelatin in 0.1 M phosphate buffer, and centrifuged to obtain a pellet (Martin and Parton, 2008). The supernatant was then removed and cells were resuspended in warm 10% gelatin, centrifuged, and left on ice to harden. Once solid, cells embedded in gelatin were trimmed into cubes that could be mounted onto specimen stubs then placed in polyvinylpyrrolidone sucrose overnight at 4°C for cryo-protection. Gelatin blocks were mounted on specimen stubs and quickly immersed in liquid N_2 ready for sectioning. For on-section labeling of frozen sections with the GST probe, sections were labeled exactly as described below for HM20 sections. Grids were viewed in a transmission electron microscope (JEOL 1011; JEOL Ltd.), and electron micrographs were taken with a digital camera (Morada; Olympus) using Analysis software (Olympus).

Immunogold labeling of HM20 sections

Thin Lowicryl sections (60–80 nm) were cut using an ultramicrotome (UC6; Leica), picked up on Formvar carbon-coated grids, dried, and kept on ice or at 4°C until they were labeled. Immunolabeling involved inverting the grid onto a series of solutions by a modification of the method of Nixon et al., (2009; see Schieber et al., 2010). Throughout the process, 0.1 M PHEM + 137 mM NaCl, pH 6.9, replaced the standard PBS to reduce nonspecific labeling (comparison of labeling with the specific C2-GST probe and GST alone). On ice, grids were quickly washed in PHEM buffer for

2 min, then immediately incubated on a 10-µl drop of C2-GST probe (2.5 µg/ml) for 30 min, after which they were washed again in PHEM buffer (twice for 2 min) before a final 5-min fixation at room temperature with 0.1% glutaraldehyde in PHEM. At room temperature, grids were washed in PHEM for 2 min, quench solution (20 mM glycine in 0.1 M PHEM) for 10 min, and blocking buffer (0.5% FSG, 0.5% BSA, and 10 mM glycine in PHEM) for 15 min. The grids were then incubated for 30 min with rabbit polyclonal GST (final concentration = 10 µg/ml; Millipore) primary antibody (7 µl), after which they were washed in block solution twice and PHEM twice (5 min each). Secondary antibody incubation (7 µl) with 10 nm Protein A–gold (Universitair Medisch Centrum Utrecht) was also for 30 min, followed by two block washes and three PHEM washes (2 min each). The reaction was finally stabilized with 1% (wt/vol) glutaraldehyde in PHEM fixation for 5 min, then washed in water (three times for 2 min) and dried in forceps. Generally, grids were viewed without further on-grid staining, although in some cases a brief UA/lead citrate staining was used to enhance contrast.

Online supplemental material

Fig. S1 shows endosomal localization of the expressed PS-binding probe. Fig. S2 shows a comparison of Tokuyasu frozen sections and HPF/FS/LTE sections labeled with the PS probe. Fig. S3 shows HPF/FS/LTE sections of adipocytes labeled with the PS probe, Fig. S4 shows light microscopic localization of the expressed PS probe to Golgi subcompartments. Fig. S5 shows the uncolored original images from Figs. 2 and 4. Online supplemental material is available at http://www.jcb.org/cgi/content/full/jcb.201012028/DC1.

This work was supported by Canadian Institutes of Health Research (CIHR) grants 7075 and MOP4665 (to S. Grinstein) and by grants from the National Health and Medical Research Council of Australia (to R.G. Parton, number 511005). G.D. Fairn is the recipient of a CIHR postdoctoral fellowship. S. Grinstein is the current holder of the Pitblado Chair in Cell Biology. L. Kuerschner was supported by postdoctoral fellowships from the Deutsche Forschungsgemeinschaft and The University of Queensland.

Submitted: 6 December 2010
Accepted: 23 June 2011

References

Ardail, D., F. Lerme, and P. Louisot. 1991. Involvement of contact sites in phosphatidylserine import into liver mitochondria. *J. Biol. Chem.* 266: 7978–7981.

Bastiani, M., and R.G. Parton. 2010. Caveolae at a glance. *J. Cell Sci.* 123:3831–3836. doi:10.1242/jcs.070102

Bastiani, M., L. Liu, M.M. Hill, M.P. Jedrychowski, S.J. Nixon, H.P. Lo, D. Abankwa, R. Luetterforst, M. Fernandez-Rojo, M.R. Breen, et al. 2009. MURC/Cavin-4 and cavin family members form tissue-specific caveolar complexes. *J. Cell Biol.* 185:1259–1273. doi:10.1083/jcb.200903053

Bell, R.M., L.M. Ballas, and R.A. Coleman. 1981. Lipid topogenesis. *J. Lipid Res.* 22:391–403.

Bishop, W.R., and R.M. Bell. 1985. Assembly of the endoplasmic reticulum phospholipid bilayer: the phosphatidylcholine transporter. *Cell*. 42:51–60. doi:10.1016/S0092-8674(85)80100-8

Chen, C.Y., M.F. Ingram, P.H. Rosal, and T.R. Graham. 1999. Role for Drs2p, a P-type ATPase and potential aminophospholipid translocase, in yeast late Golgi function. *J. Cell Biol.* 147:1223–1236. doi:10.1083/jcb.147.6.1223

Cui, Z., J.E. Vance, M.H. Chen, D.R. Voelker, and D.E. Vance. 1993. Cloning and expression of a novel phosphatidylethanolamine N-methyltransferase. A specific biochemical and cytological marker for a unique membrane fraction in rat liver. *J. Biol. Chem.* 268:16655–16663.

de Silva, A., I. Braakman, and A. Helenius. 1993. Posttranslational folding of vesicular stomatitis virus G protein in the ER: involvement of noncovalent and covalent complexes. *J. Cell Biol.* 120:647–655. doi:10.1083/jcb.120.3.647

Dominski, J., L. Binaglia, H. Dreyfus, R. Massarelli, M. Mersel, and L. Freysz. 1983. A study on the topological distribution of phospholipids in microsomal membranes of chick brain using phospholipase C and trinitrobenzenesulfonic acid. *Biochim. Biophys. Acta*. 734:257–266. doi:10.1016/0005-2736(83)90123-2

Dowler, S., G. Kular, and D.R. Alessi. 2002. Protein lipid overlay assay. *Sci. STKE*. 2002:pl6. doi:10.1126/stke.2002.129.pl6

Downes, C.P., A. Gray, and J.M. Lucocq. 2005. Probing phosphoinositide functions in signaling and membrane trafficking. *Trends Cell Biol.* 15:259–268. doi:10.1016/j.tcb.2005.03.008

Gagescu, R., N. Demaurex, R.G. Parton, W. Hunziker, L.A. Huber, and J. Gruenberg. 2000. The recycling endosome of Madin-Darby canine kidney cells is a mildly acidic compartment rich in raft components. *Mol. Biol. Cell*. 11:2775–2791.

Graham, T.R., and M.M. Kozlov. 2010. Interplay of proteins and lipids in generating membrane curvature. *Curr. Opin. Cell Biol.* 22:430–436. doi:10.1016/j.ceb.2010.05.002

Greenfield, J.J., and S. High. 1999. The Sec61 complex is located in both the ER and the ER-Golgi intermediate compartment. *J. Cell Sci.* 112: 1477–1486.

Henson, P.M., and D.A. Hume. 2006. Apoptotic cell removal in development and tissue homeostasis. *Trends Immunol.* 27:244–250. doi:10.1016/j.it.2006.03.005

Herrmann, A., A. Zachowski, and P.F. Devaux. 1990. Protein-mediated phospholipid translocation in the endoplasmic reticulum with a low lipid specificity. *Biochemistry*. 29:2023–2027. doi:10.1021/bi00460a010

Higgins, J.A., and R.M. Dawson. 1977. Asymmetry of the phospholipid bilayer of rat liver endoplasmic reticulum. *Biochim. Biophys. Acta*. 470:342–356. doi:10.1016/0005-2736(77)90126-2

Hua, Z., P. Fatheddin, and T.R. Graham. 2002. An essential subfamily of Drs2p-related P-type ATPases is required for protein trafficking between Golgi complex and endosomal/vacuolar system. *Mol. Biol. Cell*. 13:3162–3177. doi:10.1091/mbc.E02-03-0172

Keenan, T.W., and D.J. Morré. 1970. Phospholipid class and fatty acid composition of golgi apparatus isolated from rat liver and comparison with other cell fractions. *Biochemistry*. 9:19–25. doi:10.1021/bi00803a003

Kobayashi, T., M.H. Beuchat, J. Chevallier, A. Makino, N. Mayran, J.M. Escola, C. Lebrand, P. Cosson, T. Kobayashi, and J. Gruenberg. 2002. Separation and characterization of late endosomal membrane domains. *J. Biol. Chem.* 277:32157–32164. doi:10.1074/jbc.M202838200

Kutateladze, T.G. 2010. Translation of the phosphoinositide code by PI effectors. *Nat. Chem. Biol.* 6:507–513. doi:10.1038/nchembio.390

Laulagnier, K., C. Motta, S. Hamdi, S. Roy, F. Fauvelle, J.F. Pageaux, T. Kobayashi, J.P. Salles, B. Perret, C. Bonnerot, and M. Record. 2004. Mast cell- and dendritic cell-derived exosomes display a specific lipid composition and an unusual membrane organization. *Biochem. J.* 380:161–171. doi:10.1042/BJ20031594

Lingwood, D., and K. Simons. 2010. Lipid rafts as a membrane-organizing principle. *Science*. 327:46–50. doi:10.1126/science.1174621

Liou, W., H.J. Geuze, and J.W. Slot. 1996. Improving structural integrity of cryosections for immunogold labeling. *Histochem. Cell Biol.* 106:41–58. doi:10.1007/BF02473201

Liu, K., K. Surendhran, S.F. Nothwehr, and T.R. Graham. 2008. P4-ATPase requirement for AP-1/clathrin function in protein transport from the trans-Golgi network and early endosomes. *Mol. Biol. Cell*. 19:3526–3535. doi:10.1091/mbc.E08-01-0025

Luke, M.R., L. Kjer-Nielsen, D.L. Brown, J.L. Stow, and P.A. Gleeson. 2003. GRIP domain-mediated targeting of two new coiled-coil proteins, GCC88 and GCC185, to subcompartments of the trans-Golgi network. *J. Biol. Chem.* 278:4216–4226. doi:10.1074/jbc.M210387200

Martin, S., and R.G. Parton. 2008. Characterization of Rab18, a lipid droplet-associated small GTPase. *Methods Enzymol.* 438:109–129. doi:10.1016/S0076-6879(07)38008-7

Martin, S., K. Driessen, S.J. Nixon, M. Zerial, and R.G. Parton. 2005. Regulated localization of Rab18 to lipid droplets: effects of lipolytic stimulation and inhibition of lipid droplet catabolism. *J. Biol. Chem.* 280:42325–42335. doi:10.1074/jbc.M506651200

Mironov, A.A., G.V. Beznoussenko, P. Nicoziani, O. Martella, A. Trucco, H.S. Kweon, D. Di Giandomenico, R.S. Polishchuk, A. Fusella, P. Lupetti, et al. 2001. Small cargo proteins and large aggregates can traverse the Golgi by a common mechanism without leaving the lumen of cisternae. *J. Cell Biol.* 155:1225–1238. doi:10.1083/jcb.200108073

Möbius, W., Y. Ohno-Iwashita, E.G. van Donselaar, V.M. Oorschot, Y. Shimada, T. Fujimoto, H.F. Heijnen, H.J. Geuze, and J.W. Slot. 2002. Immunoelectron microscopic localization of cholesterol using biotinylated and non-cytolytic perfringolysin O. *J. Histochem. Cytochem.* 50:43–55. doi:10.1177/002215540205000105

Muthusamy, B.P., P. Natarajan, X. Zhou, and T.R. Graham. 2009. Linking phospholipid flippases to vesicle-mediated protein transport. *Biochim. Biophys. Acta*. 1791:612–619.

Nixon, S.J., R.I. Webb, M. Floetenmeyer, N. Schieber, H.P. Lo, and R.G. Parton. 2009. A single method for cryofixation and correlative light, electron microscopy and tomography of zebrafish embryos. *Traffic*. 10:131–136. doi:10.1111/j.1600-0854.2008.00859.x

Pike, L.J., X. Han, and R.W. Gross. 2005. Epidermal growth factor receptors are localized to lipid rafts that contain a balance of inner and outer leaflet lipids: a shotgun lipidomics study. *J. Biol. Chem.* 280:26796–26804. doi:10.1074/jbc.M503805200

Plowman, S.J., C. Muncke, R.G. Parton, and J.F. Hancock. 2005. H-ras, K-ras, and inner plasma membrane raft proteins operate in nanoclusters with differential dependence on the actin cytoskeleton. *Proc. Natl. Acad. Sci. USA*. 102:15500–15505. doi:10.1073/pnas.0504114102

Prescott, A.R., J.M. Lucocq, J. James, J.M. Lister, and S. Ponnambalam. 1997. Distinct compartmentalization of TGN46 and beta 1,4-galactosyltransferase in HeLa cells. *Eur. J. Cell Biol.* 72:238–246.

Presley, J.F., N.B. Cole, T.A. Schroer, K. Hirschberg, K.J. Zaal, and J. Lippincott-Schwartz. 1997. ER-to-Golgi transport visualized in living cells. *Nature*. 389:81–85. doi:10.1038/38891

Prior, I.A., C. Muncke, R.G. Parton, and J.F. Hancock. 2003. Direct visualization of Ras proteins in spatially distinct cell surface microdomains. *J. Cell Biol.* 160:165–170. doi:10.1083/jcb.200209091

Rabouille, C., N. Hui, F. Hunte, R. Kieckbusch, E.G. Berger, G. Warren, and T. Nilsson. 1995. Mapping the distribution of Golgi enzymes involved in the construction of complex oligosaccharides. *J. Cell Sci.* 108:1617–1627.

Raiborg, C., and H. Stenmark. 2009. The ESCRT machinery in endosomal sorting of ubiquitylated membrane proteins. *Nature*. 458:445–452. doi:10.1038/nature07961

Schieber, N.L., S.J. Nixon, R.I. Webb, V.M. Oorschot, and R.G. Parton. 2010. Modern approaches for ultrastructural analysis of the zebrafish embryo. *Methods Cell Biol.* 96:425–442. doi:10.1016/S0091-679X(10)96018-4

Shao, C., V.A. Novakovic, J.F. Head, B.A. Seaton, and G.E. Gilbert. 2008. Crystal structure of lactadherin C2 domain at 1.7A resolution with mutational and computational analyses of its membrane-binding motif. *J. Biol. Chem.* 283:7230–7241. doi:10.1074/jbc.M705195200

Sherer, N.M., M.J. Lehmann, L.F. Jimenez-Soto, A. Ingmundson, S.M. Horner, G. Cicchetti, P.G. Allen, M. Pypaert, J.M. Cunningham, and W. Mothes. 2003. Visualization of retroviral replication in living cells reveals budding into multivesicular bodies. *Traffic*. 4:785–801. doi:10.1034/j.1600-0854.2003.00135.x

Shi, J., C.W. Heegaard, J.T. Rasmussen, and G.E. Gilbert. 2004. Lactadherin binds selectively to membranes containing phosphatidyl-L-serine and increased curvature. *Biochim. Biophys. Acta*. 1667:82–90. doi:10.1016/j.bbamem.2004.09.006

Simons, K., and M.J. Gerl. 2010. Revitalizing membrane rafts: new tools and insights. *Nat. Rev. Mol. Cell Biol.* 11:688–699. doi:10.1038/nrm2977

Slot, J.W., and H.J. Geuze. 2007. Cryosectioning and immunolabeling. *Nat. Protoc.* 2:2480–2491. doi:10.1038/nprot.2007.365

Sundler, R., S.L. Sarcione, A.W. Alberts, and P.R. Vagelos. 1977. Evidence against phospholipid asymmetry in intracellular membranes from liver. *Proc. Natl. Acad. Sci. USA*. 74:3350–3354. doi:10.1073/pnas.74.8.3350

Touret, N., P. Paroutis, M. Terebiznik, R.E. Harrison, S. Trombetta, M. Pypaert, A. Chow, A. Jiang, J. Shaw, C. Yip, et al. 2005. Quantitative and dynamic assessment of the contribution of the ER to phagosome formation. *Cell*. 123:157–170. doi:10.1016/j.cell.2005.08.018

Trajkovic, K., C. Hsu, S. Chiantia, L. Rajendran, D. Wenzel, F. Wieland, P. Schwille, B. Brügger, and M. Simons. 2008. Ceramide triggers budding of exosome vesicles into multivesicular endosomes. *Science*. 319:1244–1247. doi:10.1126/science.1153124

van Genderen, I.L., G. van Meer, J.W. Slot, H.J. Geuze, and W.F. Voorhout. 1991. Subcellular localization of Forssman glycolipid in epithelial MDCK cells by immuno-electronmicroscopy after freeze-substitution. *J. Cell Biol.* 115:1009–1019. doi:10.1083/jcb.115.4.1009

van Meer, G. 1998. Lipids of the Golgi membrane. *Trends Cell Biol.* 8:29–33. doi:10.1016/S0962-8924(97)01196-3

van Meer, G., D.R. Voelker, and G.W. Feigenson. 2008. Membrane lipids: where they are and how they behave. *Nat. Rev. Mol. Cell Biol.* 9:112–124. doi:10.1038/nrm2330

Vance, J.E. 2008. Phosphatidylserine and phosphatidylethanolamine in mammalian cells: two metabolically related aminophospholipids. *J. Lipid Res.* 49:1377–1387. doi:10.1194/jlr.R700020-JLR200

Vonderheit, A., and A. Helenius. 2005. Rab7 associates with early endosomes to mediate sorting and transport of Semliki forest virus to late endosomes. *PLoS Biol.* 3:e233. doi:10.1371/journal.pbio.0030233

Voorhout, W., I. van Genderen, G. van Meer, and H. Geuze. 1991. Preservation and immunogold localization of lipids by freeze-substitution and low temperature embedding. *Scanning Microsc. Suppl.* 5:S17–S24, discussion :S24–S25.

Wanaski, S.P., B.K. Ng, and M. Glaser. 2003. Caveolin scaffolding region and the membrane binding region of SRC form lateral membrane domains. *Biochemistry*. 42:42–56. doi:10.1021/bi012097n

Wollert, T., and J.H. Hurley. 2010. Molecular mechanism of multivesicular body biogenesis by ESCRT complexes. *Nature*. 464:864–869. doi:10.1038/nature08849

Wubbolts, R., R.S. Leckie, P.T.M. Veenhuizen, G. Schwarzmann, W. Möbius, J. Hoernschemeyer, J. Slot, H.J. Geuze, and W. Stoorvogel. 2003. Proteomc and biochemical analyses of human B cell-derived exosomes. *J. Biol. Chem.* 278:10963–10972. doi:10.1074/jbc.M207550200

Yeung, T., G.E. Gilbert, J. Shi, J. Silvius, A. Kapus, and S. Grinstein. 2008. Membrane phosphatidylserine regulates surface charge and protein localization. *Science*. 319:210–213. doi:10.1126/science.1152066

Yeung, T., B. Heit, J.F. Dubuisson, G.D. Fairn, B. Chiu, R. Inman, A. Kapus, M. Swanson, and S. Grinstein. 2009. Contribution of phosphatidylserine to membrane surface charge and protein targeting during phagosome maturation. *J. Cell Biol.* 185:917–928. doi:10.1083/jcb.200903020

Zachowski, A. 1993. Phospholipids in animal eukaryotic membranes: transverse asymmetry and movement. *Biochem. J.* 294:1–14.

Zinser, E., C.D. Sperka-Gottlieb, E.V. Fasch, S.D. Kohlwein, F. Paltauf, and G. Daum. 1991. Phospholipid synthesis and lipid composition of subcellular membranes in the unicellular eukaryote Saccharomyces cerevisiae. *J. Bacteriol.* 173:2026–2034.